LASER-INDUCED PLASMA SPECTROSCOPY IN THE ANALYSIS OF PHOSPHATE MINING SAMPLES AND ARCHAEOLOGICAL MATERIALS

By

MARK ANTHONY VILLORIA

A DISSERTATION PRESENTED TO THE GRADUATE SCHOOL OF THE UNIVERSITY OF FLORIDA IN PARTIAL FULFILLMENT OF THE REQUIREMENTS FOR THE DEGREE OF DOCTOR OF PHILOSOPHY

UNIVERSITY OF FLORIDA

2002

This dissertation is sincerely dedicated to my parents, Florecito Bacho Villoria and Delynn Aya-ay Villoria, who have instructed me over many years the value of an education and have equipped me with the determination to obtain one.

ACKNOWLEDGMENTS

I would like to extend sincere gratitude to Dr. Jim Winefordner for his generous support during my graduate career at the University of Florida. His environment of enormous instrumental capabilities combined with a diverse, cooperative team has encouraged much intellectual and experimental freedom. Also, special appreciation is extended to Dr. Benjamin Smith, whose sound, patient guidance and encouraging support have given much direction to my research.

I am also grateful to all past and present members of the Winefordner group for their wisdom, support, and friendship. I especially thank Dr. Igor Gornushkin for his resourcefulness and vast contributions to these investigations. I appreciate the many invaluable visiting scientists to the group, namely Dr. Jesús Anzano, Dr. Chris Stevenson, and Dr. Ga'bor Gal'bacs. Other researchers receiving special recognition include Dr. David Powell, Dr. Rolf Hummel, Lee Pearson, and Michael Stora. Apart from the laboratory, many people have contributed to the success of my graduate career. Jeanne Karably, Steve Miles, Larry Hartley, Joe Shalosky, Joseph Carusone, and Matt Glover are all appreciated for their friendships, fine workmanship, and priceless advice.

I sincerely would like to extend gratitude to those professors who have planted deep roots not only in chemistry but also in my life prior to graduate school. Dr. K. C. Nainan of Stone Mountain High School introduced me to the concepts of chemistry and challenged me through national competition during my teenage years. On the undergraduate level, Dr. Larry McRae and Dr. Barbara Mixon allowed me the freedom to

explore many intellectual pursuits and encouraged me to continue my explorations in graduate school.

My family has always been a source of encouragement. I appreciate the liberty they have given me in pursuing my goals. I am deeply indebted to my parents for their continual love and sacrifice over the years. I also am grateful for the many relationships I have formed in Gator Christian Life, people with whom I have shared my life during my graduate career. I am extremely appreciative of my wonderful fiancée, Oleah Hodge, for her encouragement and invaluable advice. Jesus Christ, my Lord and Savior, is the foundation of my faith, without Whom none of this would have ever been possible. Finally, I acknowledge the financial support of IMC-Agrico, which has funded a portion of this research.

TABLE OF CONTENTS

LIST OF TABLES

LIST OF FIGURES

Abstract of Dissertation Presented to the Graduate School
of the University of Florida in Partial Fulfillment of the
Requirements for the Degree of Doctor of Philosophy

LASER-INDUCED PLASMA SPECTROSCOPY IN THE ANALYSIS OF PHOSPHATE MINING SAMPLES AND ARCHAEOLOGICAL MATERIALS

By

Mark Anthony Villoria

May 2002

Chairman: Professor James D. Winefordner
Major Department: Chemistry

Laser-induced plasma spectroscopy (LIPS) is a versatile technique used in many academic and industrial settings. The LIPS technique is a well-established method for the rapid elemental analysis of various materials with little or no sample preparation. A laser pulse of sufficiently high power is tightly focused onto a sample surface. A hot, intense plasma is formed as the surface is heated by the laser and as material is ablated. The emitted radiation is spectrally resolved and the emitting species in the laser-induced plasma are identified. The elemental composition of the sample is then determined by its unique spectral wavelengths and line intensities.

Identification of materials is achieved by using these spectral "fingerprints" that are unique to each sample. The focus of this research is to use these fingerprints in a variety of applications. Spectral data were analyzed by linear correlation, nonparametric

rank correlation, and principal component analysis. The feasibility of using these chemometric techniques in LIPS was compared.

Several studies involved the development and evaluation of various instrumental configurations, with the goal of optimizing a configuration for use in the phosphate industry. This research will discuss the development of field instruments that help to minimize contamination of matrix material (phosphate ore) by overburden or bedrock material through rapid field identification. Research has demonstrated the feasibility of accurately identifying material in its untreated, natural state with no sample preparation. The application of LIPS involves acquiring spectra of several selected samples, developing a library from these spectra, and using a correlation technique to match unknown spectra with well-characterized library spectra. Software was developed to rapidly carry out the correlation procedure and display material identification.

Furthermore, LIPS was used to study the archaeological significance of certain ceramics from the first century BC. Finally, the analytical matrix effects commonly found in LIP spectra were investigated.

CHAPTER 1
INTENT AND SCOPE OF DISSERTATION

It is the author's impression that the direction of graduate research does not always follow the path for which it was initially intended. Such is the case with the graduate career of the author. The original focus of a couple of years of research was the investigation of silicon surfaces in a new field known as Desorption/Ionization on Silicon Time-of-Flight Mass Spectrometry. However, the direction of research changed when financial support of IMC-Agrico became available. Thus, this dissertation represents only the research conducted in laser-induced plasma spectroscopy (LIPS) and does not include research involving mass spectrometry.

Chapter 2 provides a brief overview of the LIPS technique, including an explanation of the theory, instrumental design, and applications. Some of the theories associated with statistical analyses, such as linear and rank correlation and principal component analysis, are explained in Chapter 3. Chapter 4 presents background information about the phosphate mining process relevant to the industrially driven research and includes the development and evaluation of different LIPS configurations for phosphate analysis. The following two chapters report on collaborative projects with Jesús Anzano, a visiting professor from the University of Zaragoza in Spain. Chapter 5 reports the investigations on the analysis of archaeological materials by LIPS. This comprises experiments dealing with both qualitative and quantitative analyses of ancient pottery samples. Chapter 6 presents studies on the matrix effects in LIPS analyses.

Finally, conclusions are presented in Chapter 7. An operational manual for the LIPS field instrument is included in the Appendix.

CHAPTER 2
INTRODUCTION TO LASER-INDUCED PLASMA SPECTROSCOPY

Laser-induced plasma spectroscopy (LIPS) has enjoyed recent popularity as an analytical technique. Many research groups have realized the potential of LIPS, resulting in an ever-increasing number of publications. The reason for this success is perhaps the wide applicability of the technique as a method for elemental analysis. In the thirty years or so since its conception, thorough research has been conducted in academic, industrial, and government laboratories in an effort to comprehend its effectiveness in a variety of applications.

The development of LIPS started in the early 1960's when Brech and Cross first demonstrated the possibility of using lasers as excitation sources in atomic emission spectroscopy [1]. By using a pulsed ruby laser and a pair of electrodes, they recorded a spectrum of elemental components in a microplasma following laser ablation. Soon afterwards, Runge et al. used a giant pulsed ruby laser to produce spectra from the coincident vaporization and excitation of metals and nonmetals [2]. Experiments showed that a breakdown of air occurred when laser radiation was brought tightly into focus. The purpose of these early experiments and others was to determine the mechanisms that led to this breakdown and to study the influence of various parameters (e.g., wavelength, focal diameter, pressure, pulse length, material) on breakdown thresholds [3].

Early instruments employed ruby or Nd:glass laser systems, a microscope for positioning and focusing the laser beam, graphite electrodes for additional excitation, and large spectrometers with photographic plates as emission detectors [4]. A summary of

these systems is given in Table 2-1. These designs, however, suffered from poor precision due to laser instability and an inadequate spectral detection system. Improvements were made in the substitution of photographic plates with photomultipliers, and later charge-coupled devices (CCDs) and charge injection devices (CIDs) [4]. The evolutionary development of the LIPS apparatus incorporates such advances in optical detection and in laser technology. Due to the achievements of conventional atomic spectroscopy techniques such as atomic absorption spectroscopy and inductively coupled plasma optical emission spectroscopy, it was not until the 1980's that LIPS began to find widespread use in chemical analysis [5]. Presently, with the advances in laser technology, LIPS has become reliable, versatile, and readily available at a low cost. The present design complements the advantages of almost no sample preparation, the analysis of all states of matter, and its capability of simultaneous multi-element detection.

Basic Principles

In LIPS, a form of atomic emission spectroscopy, a high-power density laser pulse is focused onto a target material. A small portion of the sample is vaporized, and a hot plasma develops. The emitted radiation from the short duration plasma is collected by a spectrometer and analyzed for elemental composition.

Ahmad and Goddard indicate five steps in the LIPS process: heating, melting, vaporization, excitation, and ionization [6]. As the laser pulse strikes the surface of a solid sample, an initial heating causes the temperature of the surface to rise to thousands of degrees. The surface responds by melting, and a small portion is vaporized into an ionized gas. In order to form this ionized gas, the metal from the surface is oxidized by

the loss of electrons. There are two main mechanisms in which the ionized metal may be formed [3] :

(eqn. 1) $e^- + M \rightarrow 2e^- + M^+$ Electron ionization

(eqn. 2) $M + mhv \rightarrow M^+ + e^-$ Multiphoton ionization .

In electron ionization (eqn. 1), electrons absorb laser radiation, and then collide with the neutral metal to ionize the solid which forms a gas. The electrons must acquire an energy greater than the band gap of the solid (or the ionization energy of the gas). Consequently, the electron concentration increases exponentially with time throughout the lifetime of the laser pulse, leading to a cascade breakdown.

Multiphoton ionization (eqn. 2) is characterized by the absorption of multiple photons by an atom or molecule. When the energy of these photons is sufficient to eject an electron from the valence to the conduction band of the solid, a metal ion and an electron result. This electron, in turn, can react with neutrals to again ionize the metal (eqn. 1).

Thus, electrons that absorb the photons undergo many collisions with themselves as well as with surrounding atoms. The energy absorbed by the electrons is distributed and passed on to the metal lattice. Once in the lattice, the energy is instantaneously converted to heat, causing a rapid rise in the surface temperature of the material, ultimately resulting in vaporization. For evaporation to occur, the energy deposited in the layer of molten metal must be greater than the latent heat of vaporization of the target, L_v (J/g) [5]. Thus, no evaporation occurs below the minimum absorbed irradiance, F_{min} (typically 10^{12} W/m^2 for a Q-switched laser). The two are related in the following equation:

(eqn. 3) $F_{min} = \rho L_v a^{1/2} t_e^{-1/2}$

where ρ is the mass density of the target (g/mm^3), a is the thermal diffusivity (mm^2/s), and t_e the duration in seconds of the laser pulse.

Equation 3 shows the dependence of the vaporization threshold on the duration of the laser pulse. Vaporization does not result from high power short pulses, whereas longer, lower power pulses produce deep holes in the target. Accordingly, an equation has been derived which relates the time of vaporization, t_v (s), to the irradiance of the laser, F (W/cm^2):

$$\text{(eqn. 4)} \qquad t_v = \frac{\pi K \rho C (T_v - T_o)^2}{4F^2}$$

where K is the thermal conductivity (J/s cm K), ρ is mass density (g/cm^3), C is heat capacity per unit mass (J/g K), and T_v and T_o are the vaporization and initial temperatures in Kelvin, respectively. This equation is used to estimate the surface temperature, depth vaporized, or the time taken to reach the boiling temperature when irradiance is close to the threshold value [5].

Once the vaporization is established at the sample surface, gas dynamic processes govern the behavior of the plasma. These processes are based on the two assumptions that the laser beam is always spatially and temporally uniform within its extent and duration, and that the molten material ejected is negligible compared with atomic ejection [6].

As the plasma is formed, the vapor pressure increases, thus affecting the laser absorption. The weakly ionized plasma is partially transparent to the laser beam, allowing direct heating of the target surface to continue. The inverse Bremsstrahlung process heats primarily the electrons, which consequently increase the plasma temperature and electron density [3]. At high laser powers, the number density of

electrons increases to a point (critical electron density), which makes the plasma opaque, preventing the laser from reaching the underlying target. (If the laser radiation has a wavelength greater than the plasma wavelength, λ_p, light is reflected and the plasma shrinks instead of expands, as it is no longer absorbing the light. The plasma wavelength is defined by $\lambda_p \approx 3.35 \times 10^7 (n_e)^{-½}$, where n_e is the electron density in the partially ionized layer.) Heating of the surface continues only indirectly by thermal conduction from the plasma. Figure 2-1 shows the absorption processes that occur as the surface is ablated.

Laser heating of the plasma continues as the plasma plume grows toward the laser [7]. The plasma thus rapidly heats and expands. Therefore, the laser is no longer heating the surface, only heating the already vaporized sample. As the plasma expands, its volume increases, reducing the density of the plasma. This decrease in density allows the laser radiation to once again penetrate the surface of the sample, causing vaporization. The cycle of vaporization, heating, and expansion is repeated throughout the laser pulse [5].

Expansion of the plasma allows interaction with the surrounding atmosphere. This atmosphere may be simply the ambient gas that existed before the laser pulse, or in the case of a vacuum, it may be the neutral gas species resulting from the escape of fast ions [3]. The ablated material, in the form of particles, free electrons, atoms, and ionized atoms, expands at a velocity much faster than the speed of sound and forms a shock wave in the surrounding atmosphere. Behind the shock wave is a region of the shock-heated ambient gas followed by the expanding plasma [3]. Figure 2-2 illustrates the interactions between the plasma and the atmosphere.

After several microseconds, collisions with ambient gas slow down the plasma plume, and the shock wave detaches from the plasma front. Plasma temperatures in the range of 10^4 to 10^5 K and electron densities on the order of 10^{15} to 10^{19} cm^3 have been measured [8]. The plasma then decays through radiative quenching and electron-ion recombination processes that lead to formation of high-density neutral species in the post-plasma plume. Decay ends with the formation of clusters and with the thermal and concentration diffusion of species into the surrounding gas. The emitted radiation (integrated over the first tens of microseconds) is spectrally resolved, and the emitting species in the laser-induced plasma are identified and quantified by their unique spectral wavelengths and line intensities.

The LIPS plasma is similar to those plasmas used in the conventional atomic emission methods such as electrode spark, arc, and inductively coupled plasma. These techniques require the sample to be placed into a plasma for excitation and emission. The LIPS plasma, however, is formed from the sample and therefore contains the desired metal. Figure 2-3 provides a visual summary of the stepwise evolution of the plasma, as well as an approximate time scale for each event.

Design Considerations

Many LIPS designs have been proposed and used successfully in a variety of applications. Some even incorporate portable capabilities for field analysis, as discussed in Chapter 4. Each of these systems consists of two major parts, one for production of the plasma and another for analysis of the radiant emission from the plasma. Plasma production usually incorporates a pulsed laser, a radiation delivery system, the target, and a movable stage for the sample. The emitted radiation is analyzed using collection optics,

a dispersion system, a detector, and a computer for control, data acquisition, and analysis. A simplified LIPS system is shown in Figure 2-4.

In order to generate the plasma, the laser must generate pulses of sufficient power. Such suitable lasers include solid state lasers, gas lasers (CO_2 and excimer), and Nd:YAG pumped- and flashlamp pumped-dye lasers [3]. Table 2-2 presents a general comparison of these three types of lasers.

Solid state lasers, such as Nd:YAG lasers, are commonly used in LIPS analyses because of their good output reproducibility, compactness, and high irradiance [5]. The fundamental wavelength of 1064 nm is the most widely used, although frequency doubled (532 nm), tripled (355 nm), and quadrupled (266 nm) wavelengths have also been successful. A Nd:YAG laser is a solid state laser composed of Nd^{3+} ions in an yttrium-aluminum-garnet host [9]. A Q-switch mode is responsible for the laser pulse. In this mode, the cavity of the laser is only switched on after the population inversion has been allowed to grow greater than the threshold value. By switching on the cavity past the threshold, the laser emits a very robust pulse [10]. This laser provides a reliable pulse (~10 ns) with an energy between 10 – 100 mJ. It has a small beam divergence allowing for efficient focusing and a choice of operation wavelengths [11].

To produce a sufficiently high power density, the laser is focused to a spot size of about 1 mm^2 by means of a spherical lens [12]. An XYZ translation stage moves the target. The stage allows movement of the sample between laser pulses, allowing fresh sample surface to be exposed for each pulse. The emitted radiation from the plasma is collected and dispersed by the spectrometer and quantified by the detector. A black box set-up of a typical LIPS apparatus can be seen in Figure 2-4.

As the laser pulse is emitted from the laser cavity, two processes occur. The plasma is formed and an array detector detects the laser pulse. The plasma shown in Figure 2-2 consists of three primary regions: the high temperature core, the lower temperature middle, and the expanding shock wave discussed above. Under atmospheric conditions, the total volume occupied by the plasma is about 3 mm^3 and its lifetime is approximately 50 microseconds. The photodiode, connected to the photodiode arrary (PDA), triggers the detector to begin recording specta.

Figure 2-5 shows the decay of the lead emission spectra observed upon analysis of a lead containing sample. In this case, over a 14 μs interval, emission signals rise to a maximum and then begin to decay. Thus, the use of gated detection allows optimization of the signal to noise ratio. Usually, light emitted only 5 – 20 μs after plasma formation is detected [13]. The ideal time delay is crucial as a discrimination between the background produced by the Bremsstrahlung continuum and the emission lines of the sample must be made [14].

Light is collected and directed to the detection system using a fiber optic cable. In some cases, a lens is used to focus the emitted light onto the end of the fiber optic [10]. By using a fiber optic to collect light, sensitivity of detection to spark position is reduced because of the large acceptance angle of the fiber [15]. In addition, the fiber optic allows the detection system to be positioned remotely from the plasma emission.

The fiber optic transfers the collected emission to narrow pass filters, a monochromator, or a spectrograph. The composition of the sample and the application determine which device is most appropriate for analysis. The spectrally resolved light is then detected using either a photomultiplier tube (PMT) or an array detector. The PMT is used to monitor a particular emission line, while the array detector allows for a

continuous recording of the spectrum [10]. Finally, a computer records the line intensities for further analysis.

Applications

There are several attractive features inherent to LIPS. A summary of these, as well as disadvantages, is given in Table 2-3. One of the most attractive characteristics is its capability in the remote sensing and process monitoring areas, possible since only optical access to the sample is required. Another attractive feature is its simultaneous multi-element capability with minimal, if any, sample preparation. There is usually no sample preparation, which eliminates the need for tedious and time-consuming sample digestion and preparation procedures. This increases throughput, since the analyte signal is not reduced by dissolution or contaminated with chemical reagents. This advantage is extremely important in the analysis of phosphate samples (Chapter 4). However, some severe problems, such as variable mass ablation, must be overcome before the technique can reach its full potential. Other problems to consider include sample heterogeneity, particle size, and the effect of moisture on samples.

LIPS has applications in numerous fields, including biology, the environment, geology, metallurgy, and nuclear industry, to name just a few. New applications are continually being discovered, and a comprehensive review on all applications is virtually impossible. Here, a few examples are briefly discussed to survey the wide applicability of the technique.

The detection of almost 20 elements present in biological fluids such as serum and blood was shown to be possible by Loree [16]. Reported levels were as low as 50 ng/ml. Radziemski et al. have used LIPS for the direct detection of dangerous elements (chlorine, fluorine, and beryllium) in the atmosphere [17]. Other environmental

applications include those of the Cremers group and Ciucci et al. The former group evaluated their instrument for the analysis of metal in soils, paints, and particles collected on filters [12], while the latter used the detection of dangerous soil pollutants to estimate the sensitivity of the technique [14].

In metallurgy, the characterization of impurities and the inhomogeneity of nominally pure metal, such as in corroded materials, is extremely important [5]. *In-situ* analysis of metals in their operation area, such as at a nuclear reactor, is also an important measurement. One group used fiber optics for remote measurements of elemental traces in the hostile environment of nuclear reactor buildings [11, 18].

Obvious chemical applications include surface analysis and depth profiling. Surface analysis is achieved by altering the position of the target as described above. Since the technique is minimally destructive, LIPS has been used in the pigment identification of painted artworks [19]. In depth profiling, successive laser pulses are shot at a stationary target, and the spectrum is recorded as material is ablated [5].

Table 2-1. Early laser systems.

Manufacturer	Model No.	Laser type (wavelength)	Year of manufacture
Thermo Jarrell Ash (Franklin, MA)	Mark I	Ruby (694.3 nm)	1963
	Mark II	Nd:glass (1060 nm)	1966
LOMO (Leningrad, Russia)	MSL 2	Nd:glass (1060 nm)	1967
Shimadzu (Tokyo, Japan)		Ruby (694.3 nm)	1967
CISE Segrate Milano (Milan, Italy)	CISE I	Ruby (694.3 nm)	1966
Ford Motor Co. (Dearborn, MI)			1963
VEB Carl Zeiss (Jena, Germany)	LMA	Nd:glass (1060 nm) or Ruby (694.3 nm)	1964
	LMA I	Nd:glass (1060 nm)	1965
Optical Technology, Inc.	Model 120	Nd:glass (1060 nm)	1965
	Model 190	Nd:glass (1060 nm)	1968

Source: [4]

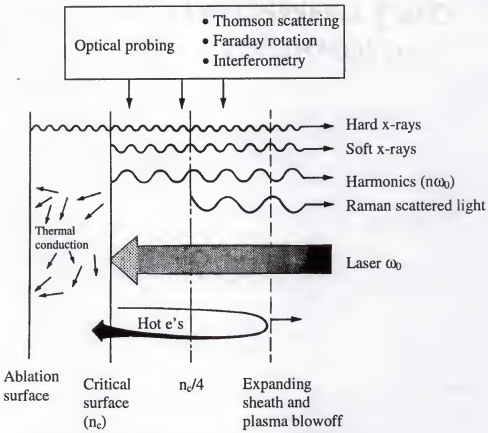

Figure 2-1. Laser plasma interaction and absorption [3].

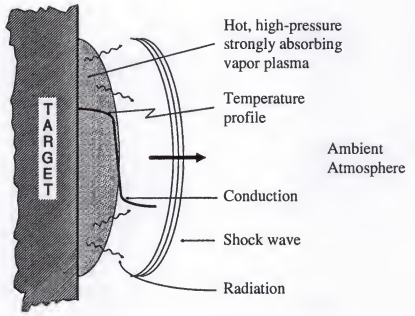

Figure 2-2. Interaction of the plasma with the ambient atmosphere [3].

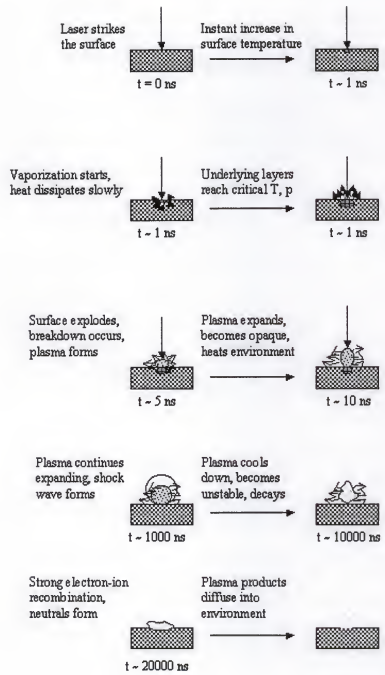

Figure 2-3. Evolution of a laser-induced plasma.

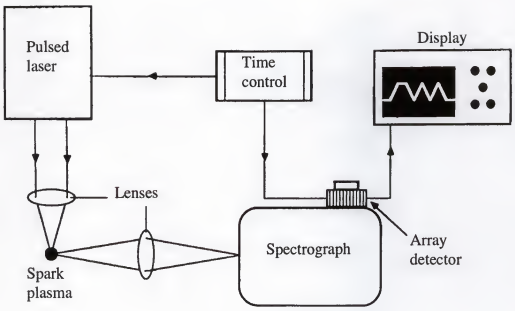

Figure 2-4. Typical LIPS set-up [3].

Table 2-2. Comparison of lasers utilized in LIPS systems.

Type	Wavelength (μm)	Pulse width (nsec)	Pulse energy (J)	Comments
Nd:YAG	1.06 0.53	7-12	0.3 to 1.0	Compact, low maintenance, reasonably priced, glass optics
CO_2	10.6	1 to 300 μsec	0.5 to 500	Simple design, inert gas, special IR optics required for laser pulses
Excimer	0.194 to 0.351	10 to 30	0.25	Rep rates to 250 Hz, UV wavelengths, toxic gases, quartz optics required for laser pulses

Source: [3]

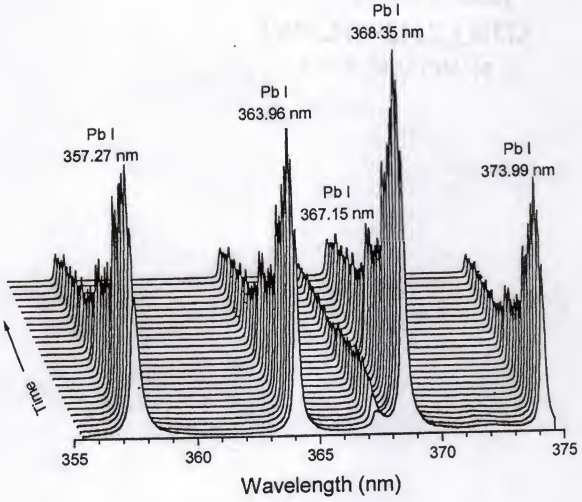

Figure 2-5. Temporal development of a series of lead emission lines in a LIPS plasma.

Table 2-3. Advantages and disadvantages of laser-induced plasma spectroscopy.

Advantages	Disadvantages
1. Minimal or no sample preparation	1. Variation in the mass ablated caused by changes in the bulk matrix
2. All states of matter can be analyzed, as well as both conductive and nonconductive samples	2. Difficulty in obtaining matrix matched standards
3. Very small amounts of material are vaporized	3. Detection limits higher than standard solution techniques (e.g. ICP – OES)
4. Easy analysis of refractory materials such as ceramics	4. Poor precision, typically 5 – 10%
5. Microanalysis is possible with spatial resolving powers of 1 – 10 μm	5. Standard emission disadvantages, such as spectral interferences and self-absorption
6. Capability of remote analysis in harsh environments	6. Possibility of optic damage from high energy density lasers
7. Atomization and excitation are in one step	7. Complexity of the operation of the system
8. Capable of simultaneous multi-element analysis	

CHAPTER 3
CHEMOMETRIC APPROACH TO LIPS

Experimental data in this dissertation were analyzed using three different statistical methods: linear correlation, nonparametric rank correlation, and principal component analysis. Linear and rank correlations were each used extensively in the identification of numerous samples because of the familiarity of these techniques with laser-induced plasma spectra [20]. LIPS is often used to identify the elemental composition of materials by the presence of one or more spectral lines in the sample's emission spectrum. Although a detailed chemical composition could be obtained, the goal of this work was to use a material's spectrum as a "fingerprint" for instant identification of that material. This fingerprint is a LIP spectrum that is compared to many other spectra in a spectral library. Each material has its own unique fingerprint, thus giving a unique positive identification of that material.

The primary objective of these statistical methods is to identify a compound belonging to a known class of compounds stored in a certain spectral library. A probe spectrum can be sequentially superimposed with the library spectra and the difference or similarity will immediately show up even without the use of a computer. In many cases, however, visual identification is not obvious, especially in transition regions. The spectra may look close to identical. Thus, powerful statistical methods are required in order to reliably identify such materials.

Goals for the qualitative identification of the compounds investigated included the rapid identification of material without extensive, laborious calculation. The

incorporation of the statistical method into customized software was critical. This was especially important for those samples used in the phosphate industry, as the software was integrated into a unique instrument adapted for rapid field analysis (as discussed in Chapter 4).

The correlation methods of choice, then, were linear correlation and nonparametric rank correlation, for these were most suitable for compound identification. The choice of correlation method is determined by the particular experimental arrangement, the type of data obtained, and time requirements [20]. In this research, linear and nonparametric rank correlation were completely adequate for spectral identification of each sample spectrum, which consists of 2048 data points. The potential of using another statistical method, principal component analysis, with LIPS data was also briefly investigated.

With the various instrumental configurations described in Chapter 4, spectra of several selected samples were acquired and used to compile the LIPS spectral libraries. A correlation technique was used to match unknown spectra with well-characterized library spectra. Software was developed to perform the correlation algorithm, rapid data processing, and simple spectrometer operation.

Linear Correlation

Linear correlation (also known as Pearson product moment correlation, or more simply, Pearson's correlation) measures the association between variables. The correlation between two variables reflects the degree to which the variables are related. The goal of a simple linear correlation is to determine whether a change in one of the independent variables is associated linearly with a change in the other independent variable. The linear correlation coefficient r is calculated as:

$$r = [\ \Sigma (X_i - X)(Y_i - Y)\ ] / [\ \Sigma (X_i - X)^2 \Sigma (Y_i - Y)^2\ ]^{1/2}$$

where X is the mean of X_i's, and Y is the mean of Y_i's. A value of r = 0.0 indicates no linear relationship between the two variables and that these two variables are uncorrelated. However, a value of +1.0 signifies a perfect positive linear relationship between variables. This complete positive correlation occurs when the data points lie on a perfect straight line with the positive slope; high values on the x axis (wavelength) are associated with high values on the y axis (spectral intensity).

As an example, in the phosphate rock samples, spectral libraries were compiled from the various types of material that could be examined. The spectral intensities of a new sample spectrum were plotted against the spectral intensities of those spectra in the library (Figure 3-1). The algorithm determines the closest match by using the above equation, and the new sample is identified as the material in the library that has the highest correlation coefficient. Practically, this is the spectrum that the new sample most closely resembles.

Rank Correlation

The linear correlation coefficient r does not take into account the individual distributions of x and y. Hence, the linear correlation coefficient r is not the most accurate statistic for deciding whether an observed correlation is statistically significant. This is especially important in this research, since fluctuating single-shot spectra (x's with different distributions) are often compared with stable library spectra (y's with similar distributions) [20]. Nonparametric rank correlation (also known as Spearman's rank correlation) is likely to be more robust since the numbers are drawn from a perfectly known distribution function.

Nonparametric rank correlation can be applied to compare two independent random variables. Unlike the linear correlation, nonparametric rank correlation works on ranked data, rather than directly on the data itself. It is with ranking (or relative) measurements, as opposed to linear measurements, that the nonparametric rank correlation method is used to analyze data. Similar to the linear correlation coefficient *r*, the Spearman's *r* coefficient indicates agreement. A value of *r* near one indicates good agreement; a value near zero implies poor agreement. Because of its dealings with ranked data, nonparametric rank correlation does not make any assumptions about the distribution of the underlying data [21].

The nonparametric rank correlation method assigns a rank to each observation in each group separately. Each value in a spectrum is replaced with the value of its rank, an integer between 1 and 2,048 in accordance with its magnitude [20]. Thus, the most intense pixel in a spectrum is assigned the number 2,048, since there are 2,048 data points (or pixels) in the spectrometer. The resulting list of numbers is drawn from a perfectly known distribution function, namely, uniformly from the integers between 1 and 2,048. Each integer in the distribution function occurs precisely once. For this research, the ranks of the probe sample spectrum were plotted against the ranks of a spectrum stored in a spectral library (Figure 3-2). The equation for nonparametric rank correlation is the same as that of linear correlation, with the exception that the values of the *x*'s and *y*'s are replaced by their corresponding ranks *R*'s and *S*'s:

$$r = [\ \Sigma (R_i - R)(S_i - S)\ ] / [\ \Sigma (R_i - R)^2 \Sigma (S_i - S)^2\ ]^{1/2} .$$

Principal Component Analysis

Principal component analysis (PCA) is a statistical method used to break down a set of data into its most basic variations. PCA is widely used in a variety of disciplines, some of which include signal processing, statistics, and neural computing. In some application areas, PCA is also known as the Karhunen-Loeve transform, the Hotteling transform, or eigenanalysis. The PCA algorithm can be applied to sets of spectroscopic data from plasma spectra, since the spectroscopic data consist of lists of measurements made on a collection of objects.

There exists a number of objectives of principal component analysis. The first is to reduce the dimensionality of data. Reduction of dimensionality is practical if the new axes account for approximately 75% or more of the variance in a data set. Another goal is to determine linear combinations of variables. Because eigenvectors are reduced to a centered point, linear combinations to relate points (spectra) to each other may be found. Next, PCA allows the visualization of multidimensional, or multivariate, data. The variance explained by a pair of axes defining a plane can be viewed on a planar plot. Finally, PCA permits the identification of groups of spectra or of outliers. Visual inspection of a planar plot indicates objects that are grouped together, thus indicating that they belong to the same type of compound or result from the same process. Anomalous objects may also be detected, in which case they may be excluded from analysis because of the perturbation that they introduce or that analysis may require repetition.

Spectroscopic data could be classified as multivariate data. The information from a set of spectra could be organized such that each datum in the data set is identified with a point. Of a sample set of about 20 spectra, for example, one spectrum can be reduced to

a single point on a graph of much fewer (2 or 3) principal components. This reduction in the dimensionality of data aids material classification.

In the spectroscopic analysis of real samples, a spectrum may be defined not only by the elemental composition of the sample, but also by the effect of a number of variables. Constituents within the sample may interact; detection, including noise, may vary among instruments; environmental conditions may affect the baseline; samples may be prepared or handled differently. Despite these variations, however, there must always be a finite number of independent variations occurring in the spectral data. It is likely that the largest variations in the spectral set would be the changes in the spectrum due to the different concentrations of the constituents of the mixtures.

PCA breaks apart the spectral data into the most common spectral variations (factors, eigenvectors, loadings) and the corresponding scaling coefficients (scores). In any set of spectra for this research, the data is 2,048 dimensional, since there exist 2,048 pixels in each spectrum. Because of the extremely large dimensionality of this data set, it is beneficial to have this dimensionality reduced to principal components to observe groupings in the data. The detailed algorithm for determining principal components is quite extensive and can be found in the literature [22, 23].

PCA of Phosphate Mining Samples

Ninety spectra were taken of three categories of phosphate material: 30 each of bedrock, matrix, and overburden. Figure 3-3 displays the laser-induced plasma spectral averages of these three classes of phosphate mining samples. Because the differences in these samples lay in the various concentrations of its constituents, the main variation in these spectra is in the intensity of certain peaks, or, more accurately, the ratio of the intensities of distinctive peaks relative to others. The intensities of each of these spectra

were compiled in a database; the final worksheet contained a matrix of 90 x 2,048 cells (number of spectra x pixels). The principal component analysis was conducted using customized programs written in MATLAB.

A log-eigenvalue plot (Figure 3-4) can be generated to illustrate the number of principal components that may be used. Each of the points of the resulting "scree" plot indicates one spectrum. This scree plot shows a number of data points that lie along an imaginary line. The points that deviate most from this line are considered to be significant principal components. Here, about 4 to 8 principal components may be considered significant.

Figure 3-5 is a plot of scores of the first two principal components plotted against one another for 30 bedrock samples. These scores represent the maximum variation of spectra. As shown, points 2 and 3 are situated at positions farther from the rest of the points. An observation of the superimposed spectra of all 30 bedrock samples (Figure 3-6) reveals spectra 2 and 3 to contain more broad peaks than that of the remaining spectra. Thus, PCA can be used to show slight variations in spectra while still retaining important spectral information.

Principal component analyses were likewise performed on matrix and overburden spectral data. The resulting data from the similar analyses are shown in the scree plots, plots of scores, and superimposed spectra (Figures 3-7 to 3-12).

The final scree plot from all 90 spectra is presented in Figure 3-13. The plot, along with a corresponding table of eigenvalues (Table 3-1), shows the reduction in dimensionality to 7 principal components to account for 99.15% of the cumulative variance.

Discriminant function analysis is commonly used to determine which variables discriminate best between two or more groups. The basic idea underlying discriminant analysis is to determine whether groups differ with regard to the mean of a feature variable. This variable is then used to predict group membership. If discriminant function analysis is effective for a set of data, the classification of correct and incorrect estimates will yield a high percentage correct. Linear discriminant analysis was used in the classification of the phosphate spectra. Further computational analysis in MATLAB allows a two-dimensional linear discriminant function plot of all three groups of spectra (Figure 3-14). The plot shows the distinct regions for the three groups. As expected, the bedrock spectra are the most distinct, separated on the plot very noticeably. Overburden and matrix are more similar, but yet separated very well.

The goals of PCA have been accomplished with the analysis of spectra from bedrock, matrix, and overburden samples. The dimensionality of the data was reduced from a 90 x 2,048 data set to a two-dimensional data plot with 90 points. A set of eigenvectors, calculated from the original calibration data, serve as scaling factors in a linear combination of the included spectra. Finally, the resulting two-dimensional plot allows the visualization of classes of spectra.

Comparison of Chemometric Methods

Table 3-2 lists the results of linear correlation, rank correlation, and principal component analysis. Principal component analysis yields results that are considerably more accurate than that of correlation analysis. The percent error for each of these analyses was 16.7%, 17.8%, and 1.11% for linear correlation, rank correlation, and principal component analysis, respectively.

Due to the ranking process in nonparametric rank correlation, the relative magnitudes of high intensity peaks are reduced, whereas the magnitudes of low intensity peaks are enhanced. This sensitivity to background noise is one major disadvantage of nonparametric rank correlation. Another drawback is that it is slower than linear correlation, since the signal intensities (pixels) must first be rearranged (ranked) prior to the correlation. The reduction of speed, however, is only on the order of tens of seconds, at most, for analyses containing fewer than a hundred spectra.

Nevertheless, linear correlation was primarily used to conduct the research in this dissertation. Principal component analysis, while a more precise algorithm for the classification of materials, requires hours of data post-treatment. In order to accumulate the data needed for PCA, it was first necessary to combine all the spectral data into a worksheet for import into the MATLAB program. Customized programs then allowed the handling of the data that concluded in the visualization of the data from a two-dimensional discriminant functions plot. While the hours of data post-treatment may be reduced to minutes with specific, customized computer programs, the handling of massive amounts of spectroscopic data would remain an enormous computational effort. The linear and rank correlations, however, are simple, robust, and not as mathematically challenging. For the purposes of the research included here, the accuracy of these correlation methods was entirely satisfactory.

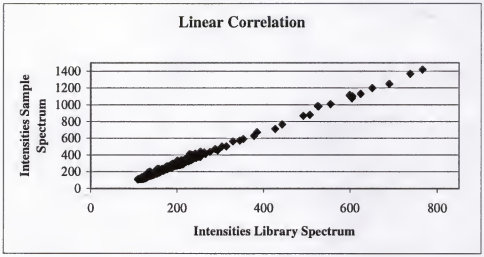

Figure 3-1. A plot of the intensities of a probe sample spectrum against the intensities of a spectrum in a spectral library.

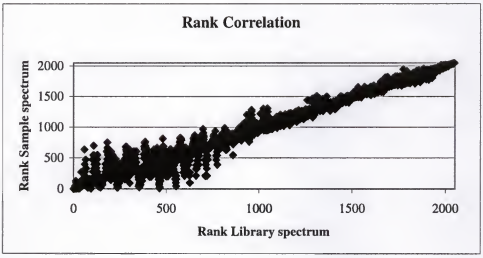

Figure 3-2. A plot of the ranks of a probe sample spectrum against the ranks of a spectrum in a spectral library.

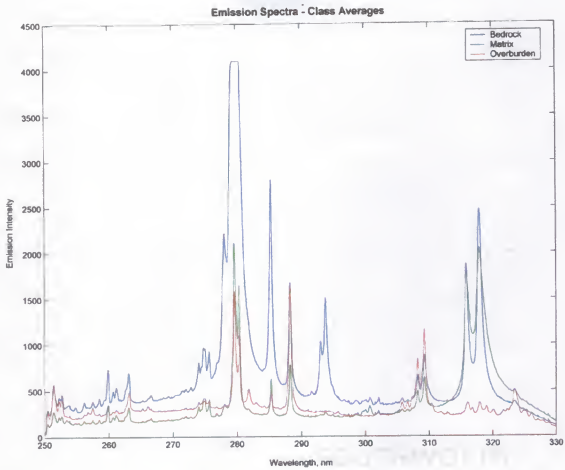

Figure 3-3. Laser-induced plasma spectral averages of three classes of phosphate mining samples: bedrock, matrix, and overburden.

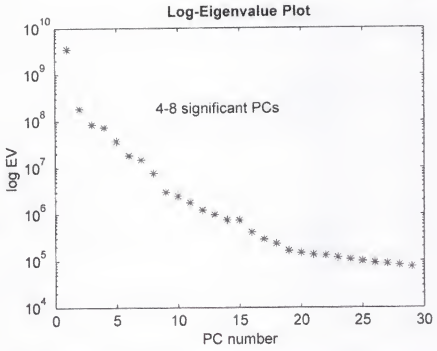

Figure 3-4. Scree plot of log-eigenvalues of bedrock principal components.

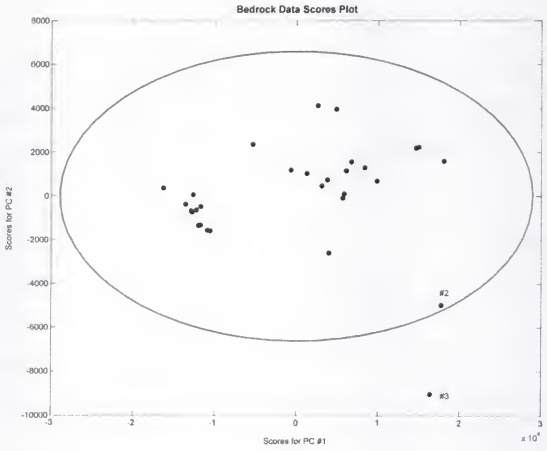

Figure 3-5. Scores of the first two principal components for bedrock spectra.

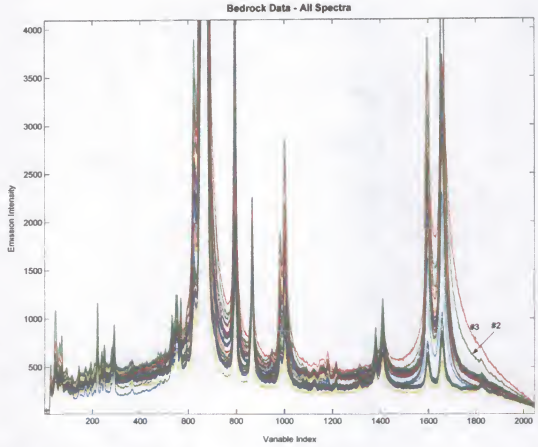

Figure 3-6. Laser-induced plasma spectra of 30 bedrock samples. X-axis is pixel number. Anomalies (#2 and #3) in spectra are easily visible.

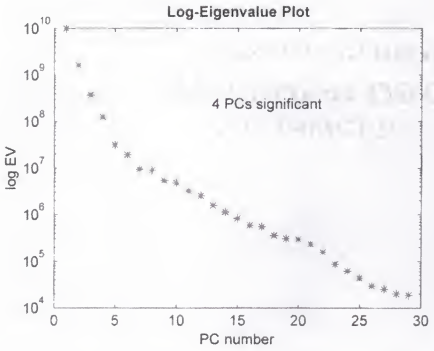

Figure 3-7. Scree plot of log-eigenvalues of matrix principal components.

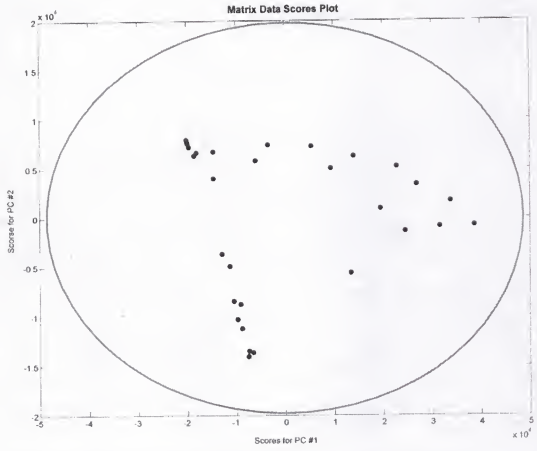

Figure 3-8. Scores of the first two principal components for matrix spectra.

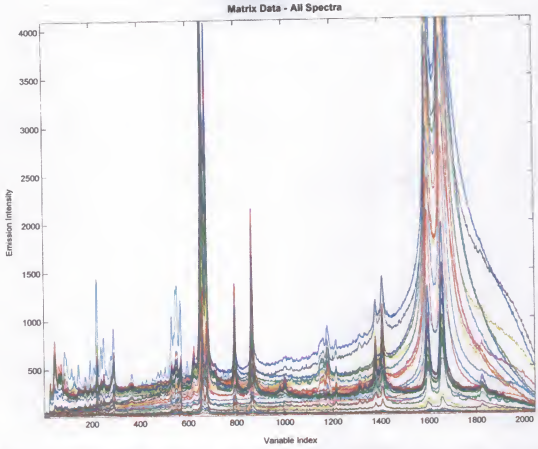

Figure 3-9. Laser-induced plasma spectra of 30 matrix samples. X-axis is pixel number. Greater inhomogeneity exists in matrix spectra.

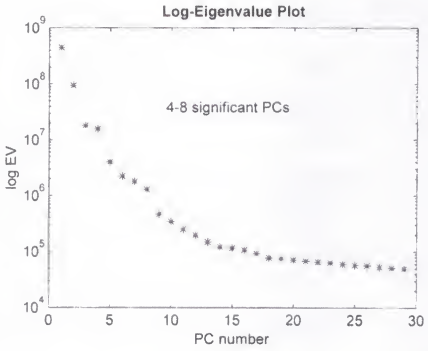

Figure 3-10. Scree plot of log-eigenvalues of overburden principal components.

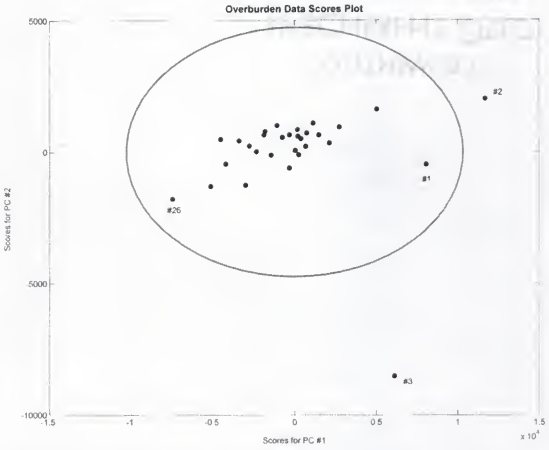

Figure 3-11. Scores of the first two principal components for overburden spectra.

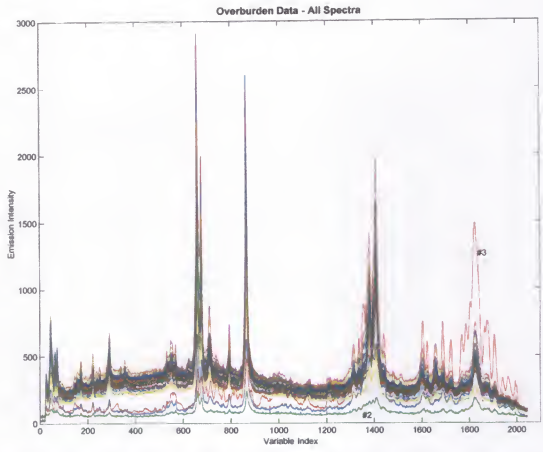

Figure 3-12. Laser-induced plasma spectra of 30 overburden samples. X-axis is pixel number.

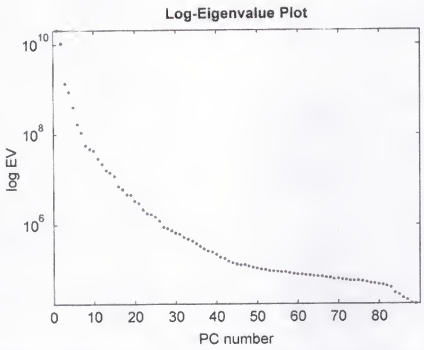

Figure 3-13. Scree plot of log-eigenvalues of principal components of three classes of phosphate mining samples.

Table 3-1. Principal components and the amount of variance each includes.

Principal Component	Eigenvalues	Variance	Cumulative Variance
1	2.04×10^{10}	59.36%	59.36%
2	1.07×10^{10}	31.14%	90.50%
3	1.39×10^{9}	4.04%	94.54%
4	8.98×10^{8}	2.61%	97.15%
5	4.05×10^{8}	1.18%	98.33%
6	1.71×10^{8}	0.50%	98.83%
7	1.12×10^{8}	0.33%	99.15%
8	5.73×10^{7}	0.17%	99.32%
9	4.77×10^{7}	0.14%	99.46%
10	4.42×10^{7}	0.13%	99.59%
11	2.96×10^{7}	0.09%	99.67%
12	2.23×10^{7}	0.06%	99.74%
13	1.59×10^{7}	0.05%	99.78%
14	1.43×10^{7}	0.04%	99.83%
15	1.20×10^{7}	0.03%	99.86%
16	7.05×10^{6}	0.02%	99.88%
17	6.03×10^{6}	0.02%	99.90%
18	4.64×10^{6}	0.01%	99.91%
19	4.59×10^{6}	0.01%	99.93%
20	3.35×10^{6}	0.01%	99.94%

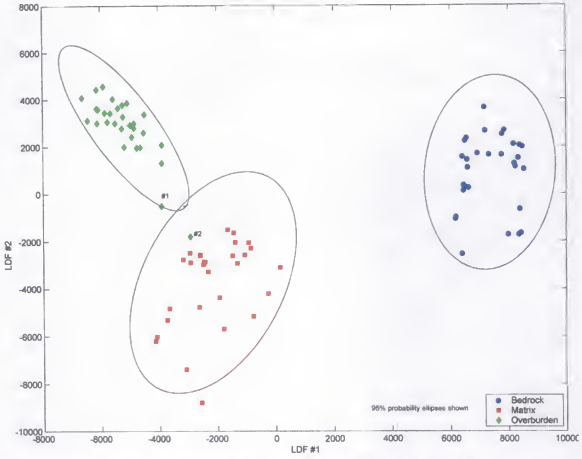

Figure 3-14. Linear discriminant analysis of bedrock, matrix, and overburden spectra.

Table 3-2. Comparison of chemometric methods.

Linear correlation: 16.7% error

Actual	*Predicted*		
	Bedrock	Matrix	Overburden
Bedrock	30	0	0
Matrix	13	16	1
Overburden	0	1	29

Rank correlation: 17.8% error

Actual	*Predicted*		
	Bedrock	Matrix	Overburden
Bedrock	30	0	0
Matrix	13	16	1
Overburden	0	1	29

Principal component analysis: 1.11% error

Actual	*Predicted*		
	Bedrock	Matrix	Overburden
Bedrock	30	0	0
Matrix	13	16	1
Overburden	0	1	29

CHAPTER 4
RAPID FIELD IDENTIFICATION OF PHOSPHATE MINING SAMPLES

The objective of this research is to develop field instruments that will help to minimize contamination of matrix material (phosphate ore) by overburden or bedrock material through rapid field identification. This project has demonstrated the feasibility of accurately identifying overburden, matrix, and bedrock material in their untreated, natural state with no sample preparation. The application of laser-induced plasma spectroscopy as described in the previous chapter involves acquiring spectra of several selected samples, developing a library from these spectra, and using a correlation technique to match unknown spectra with well-characterized library spectra. Software was developed to rapidly carry out the correlation procedure and display material identification.

In the development of field instruments for industrial applications, several experimental avenues have been explored. Identification of overburden, matrix, and bedrock samples was achieved by using four different configurations: a prototype benchtop instrument, a hand-held fiber-optic probe, the telescopic probe and finally a field LIPS probe. A review of these results is presented. Finally, a field portable instrument was designed, constructed, optimized and delivered to IMC-Agrico.

Phosphate Mining

Mining in Florida, after tourism and agriculture, is the third largest industry in the state. The mining industry and its associated industries such as the processing and shipping of minerals provide numerous employment opportunities and a wide variety of

products. About 90 percent of the rock mined is used in the production of agricultural fertilizers which are sold internationally. About 5 percent is used for livestock feed supplements, and the remainder is used for common items such as soft drinks, toothpaste, light bulbs, vitamins, and shaving cream.

The role of Florida in the phosphate industry is paramount, as it is the supplier of 75 percent of the United States' fertilizer and other phosphate needs and 25 percent of the world demand for phosphate products. Phosphate production has been an important component of the Florida economy for the past 100 years.

The production of phosphate is a two step process: (1) the mining of the raw phosphate, including cleaning and separating out impurities and (2) the processing of the phosphate to make it suitable for commercial use. The phosphate matrix, a mixture of pebbles, sand, and clay, is typically found an average of 25 feet below the surface. Overburden, the material above the matrix, is removed by large draglines. The draglines then deposit the matrix in containment wells, where high-pressure water guns liquefy material into a slurry for pipeline transport to the processing plant.

Phosphorus exists in nature with calcium, magnesium, and other elements in phosphate rock. After phosphate rock is ground to a fine and uniform size, it is reacted with sulfuric acid, releasing phosphorus as phosphoric acid, a soluble, readily available form that can be utilized by growing plants.

$$Ca_5(PO_4)_3OH(s) + 5H_2SO_4(aq) \rightarrow 3H_3PO_4(aq) + 5CaSO_4(s) + H_2O(l)$$

The phosphoric acid is concentrated, then reacted with ammonia, a source of nitrogen. The two most common products produced are diammonium phophate (DAP) and monoammonium phosphate (MAP). Other common products include fertilizers

materials such as granular triple superphosphate and urea and animal feed ingredients including calcium phosphate products.

The phosphate industry is unique in that Florida law requires that all land that is mined be reclaimed; every acre mined must be reshaped. The industry is very sensitive to environmental needs. Nearly every phosphate plant relies on the self-generation of its electricity needs, driven by the waste heat from its facilities. In addition, factories re-use over 98 percent of the water used in mining and processing. These issues address cost efficiency as well as environmental concerns.

Background

In the mechanical removal of apatite ore from the earth, it is necessary to distinguish the transitional interface between the undesirable material that lies directly above (overburden) and beneath (bedrock) the matrix layer of ore. This is traditionally done by preliminary visual examination of core samples by trained geologists, limited chemical analysis of field samples, and visual observations of the exposed mine pit by the drag line operator. The locations of these interfaces are generally not very well known due to the limited number of core samples which can be economically obtained and the uncertainties in the identification of the core sample composition. Therefore, the dragline operator must rely on approximate or extrapolated data for the depth of the overburden and matrix. This rough estimation often leads to reduced efficiency in the recovery of raw material or contamination of valuable ore with undesirable compounds such as excessive MgO from the bedrock. It would be extremely useful to have a rapid, reliable field measurement technique to accurately identify overburden, matrix, and bedrock material in core samples. This would provide far more accurate preliminary identification of the topography in the mining operation. Improvements would come

from using a larger number of sampling locations with improved depth resolution. In addition, it would be very useful for the drag line operator to have available real time measurements of the content of each load of material or of the spatially-resolved composition of the exposed surface of the mine pit. The goal of this research is to develop and evaluate an approach to solve these measurement problems using laser-induced plasma spectroscopy and thereby enhance the efficiency with which apatite ore is removed from the earth.

Preliminary studies

Figure 4-1 shows typical LIP spectra of overburden, matrix and bedrock samples in a spectral window from 240 – 340 nm. In this range, spectral lines for Si, Fe, Al and Mg can be easily observed. Several obvious compositional differences are clear. Overburden tends to have higher Si concentration, matrix tends to be relatively low in Fe and bedrock is particularly high in Mg levels. In a preliminary study, measurement indices were devised which related the ratio of these spectral lines to the individual materials. Using a measurement approach first suggested by Regis Stana, the feasibility of identifying natural soils as overburden, matrix or bedrock was tested. Unknown (blind) samples of these materials were provided by IMC-Agrico. Six samples labeled A1, A2, A3, B1, B2 and B3 were received, sealed in plastic bags in a five-gallon shipping bucket. From each sample, about 5 g of material was removed with a small scoop and pressed loosely into a small sample dish, 2.5 cm in diameter and 4 mm deep. Scraping with a microscope slide roughly leveled the surface. This single dish of soil constituted the analytical sample for each bag of material. The samples were measured wet, as taken from the original bags.

Laser-induced plasma spectra were acquired for each of the six analytical samples using the compact LIPS instrument developed previously [20]. A laser pulse energy of 50 mJ was focused with a 10 cm focal length lens resulting in a spot size at the sample surface of about 0.5 mm. For each sample, 11 or 12 runs were made, each consisting of 10 laser samplings at random points on the sample surface. Therefore, a total of 110 or 120 laser shots were averaged for each sample. The laser was operated at a repetition rate of 1 Hz. Spectra were captured through a fiber optic link to a compact Ocean Optics spectrometer. Customized software identified the spectral lines, located the background, and calculated the net line intensities for each laser shot.

Table 4-1 shows the normalized, averaged results for the six samples. Four different indices, Si/P, Si/Mg, Si/Al and Si/Fe were evaluated. The average relative uncertainties were 50%, 33%, 33% and 30%, respectively. The Si/P ratio did not vary consistently and, having the poorest precision was rejected as an indicator. The Si/Al ratio did not vary significantly among the 6 samples tested. The Si/Mg and Si/Fe ratios both showed statistically significant differences between the 6 samples with the Si/Mg ratio proving to be the most reliable indicator.

Based upon these preliminary results, a full evaluation of the method proceeded and the correlation data analysis approach was developed to use the entire content of the measured spectra rather than any particular pair of spectral lines.

Correlation Studies with the Benchtop Instrument

Experimental Setup and Methodology

The preliminary work was repeated to confirm the ability to reliably identify soils as overburden, matrix, or bedrock. Approximately 8 g of unknown samples provided by

IMC-Agrico were loosely pressed into a sample dish, 3.0 cm in diameter and 8 mm deep. A spatula was used to roughly level the surface.

Laser-induced plasma spectra were obtained from each of six samples using the configuration depicted in Figure 4-2. A laser pulse (Big Sky Laser Technologies, Inc., 1064 nm) at a repetition rate of 1 Hz and pulse energy of 50 mJ was aligned through a pierced mirror. The laser was then focused with a 15 cm focal length lens resulting in a spot size at the sample surface of about 0.5 mm. Light emitted at the sample surface was collected by the pierced mirror and focused by a lens (12 cm focal length) through a neutral density filter and onto a fiber optic cable linked to an Ocean Optics spectrometer.

For each sample, 10 runs were made, each consisting of 10 laser samplings at random points on the sample surface, resulting in 100 laser shots for each sample. The resulting spectra were averaged to form a library for each sample. Single shot spectra were obtained for random samples and compared against the libraries for identification. Spectra were obtained in the 250-330 nm spectral window. Figure 4-3 shows a typical spectrum resulting from the average of 10 laser shots.

Several samples, obtained from IMC-Agrico, were analyzed using the customized software. These same samples were also sent back to IMC-Agrico for identification by chemical analysis. The phosphorus (P_2O_5) and magnesium (MgO) content of each of the samples was obtained by wet digestion. The identification by LIPS was correlated against these analytical results obtained by IMC-Agrico.

Because it is expected to have variations in surface topography with core sampling, the effect of sample height (position relative to the laser focus) on the identification of the soils was studied. To examine this effect, spectra were acquired for

each sample at various positions above and below the focal plane of the focusing lens. The laser pulse energy was 50 mJ, the repetition rate of the laser was 2 Hz, and 10 laser shots were averaged for each sample. A library was made for each specific position from the focal plane (e.g., +/-1.0 cm from the optimum focus). Each library contained the data for each of the three layers.

Core sampling movement was simulated by the mechanical translation of a sample tray packed with overburden, matrix, and bedrock. The motorized translation stage moves at approximately 0.25 cm/s over a distance of about 18 cm. Overburden, matrix, and bedrock material were tightly packed with distinct transitions into a 5 cm x 30 cm sample tray placed on top of the translation stage. First, a correlation library was made for overburden by collecting and averaging about 30 spectra of overburden sample. Then, the translation stage and the correlation algorithm in the software were simultaneously initiated. Finally, a graph of the correlation coefficient vs. laser shot number (distance) was plotted as each spectrum was collected.

Results

The averaged correlation coefficients from the ten libraries are displayed in Table 4-2. As shown previously, the software easily distinguishes among overburden, matrix, and bedrock. As an example, the correlation coefficients for a matrix sample are graphically depicted in Figure 4-4. Correlation coefficients for both matrix samples are high, while those of other samples are significantly lower. In addition, excellent precision (standard deviation <0.06) was obtained. From the single shot spectra of random samples, we observed a high degree of confidence in classifying the soils as overburden, matrix, or bedrock. This data analysis approach could even distinguish between different samples of material within the three sample categories.

The results from chemical analyses are shown in Table 4-3. The criteria used for classifying the samples as overburden, matrix, or bedrock are shown in Table 4-4. Samples with values in between those given values in Table 4-4 would likely be obtained from the interface between two layers. The LIPS determination of the samples correlates quite well with the results obtained from chemical analysis. There are occasions when there may be a discrepancy between the two methods of identification (e.g. Sample 4). Particles of the matrix may have been embedded within the bedrock sample, giving a false identification. This error, however, would be minimized or perhaps eliminated by averaging several laser probings of each sample.

Effect of Sample Position

As expected, the manipulation of the sample height below the focusing lens showed that the highest spectral quality is observed at the focal length of the lens. Figure 4-5 shows the effect of sample distance on the correlation coefficients using the maximum laser pulse energy (50 mJ). In this figure, a spectrum taken at the lens focal length (distance = 0 cm) was used for the correlation library and the matrix spectrum is the source spectrum in each library. It is important to note that, even though the correlation coefficient was poorer out of the plane of laser focus, the sample was always identified as matrix, regardless of the sample position. Another significant observation is the difference in correlation coefficients at each specific position. Within each layer, the correlation coefficients follow the same trend: matrix, bedrock, overburden. A similar study at lower laser energy showed that the reliability of identification degrades for material closer than the lens focal length, as can be seen in Figure 4-6.

Continuous Correlation on a Moving Sample

Results from motorized sample translation are shown in Figure 4-7. Three distinct regions of correlation coefficients are apparent on the graph. The large variations in the correlation coefficients for the middle region (matrix) are likely due to inhomogeneity in the sample. Nevertheless, the resulting plot still indicates when the transitions between layers occurred and correctly identifies the 3 materials in all cases. Another alternative is to perform the correlation against the last spectrum observed, thus detecting changes in the sample composition. Another method is to correlate against each of the three libraries, which would improve the precision within any one region. These alternative algorithms may be developed and evaluated for their effectiveness and ease of identification of layers.

Fiber-Optic Probe

Experimental Setup and Methodology

The portability of this technology in the field is an obvious advantage. This avenue was explored with the design of a miniaturized LIPS probe, shown in Figure 4-8. The miniature probe measured 2 inches in diameter and was easily held in one hand (Figure 4-9). A small trigger button on the probe is connected to a customized laser trigger circuit, shown in Figure 4-10, to initiate the laser pulse. As the probe is pressed against the sample, the operator depresses the trigger button and a spectrum is immediately obtained. The laser (1064 nm) was coupled through an optical fiber to the probe head. The resulting power at the output of the optical fiber was ~40 mJ. The fiber output was focused on the sample with a ½" diameter lens, precisely located at the optimal focal distance. Emitted light from the plasma was collected by another optical fiber positioned at an angle with respect to the laser beam. The optical fiber (400 μm)

guided the light into the spectrometer (Ocean Optics, Inc.), which was interfaced to a laptop computer.

Results

The results from the fiber optic LIPS probe are shown in Table 4-5. Two hundred laser shots were used on each of the samples of known origin. Every laser shot was used in the classification of each sample. In a field setting, the poor spectra would not be used; instead, those spectra would be discarded and another spectrum taken. A threshold value could easily be set in the software, prompting the operator to repeat a measurement if the overall spectrum intensity was too low. At maximum power, an identification accuracy of 87% was achieved when all spectra were evaluated. This improves to 95% when the poor spectra are discarded.

Although this system performed adequately in the laboratory, the coupling efficiency of the laser through the optical fiber was difficult to maintain and the amount of energy delivered to the sample was about 10X lower than the system without the fiber optic link. This resulted in a much weaker plasma, requiring better sample presentation (surface uniformity, moisture content). It was therefore concluded that the field instrument design would not use a fiber optic laser link.

Remote LIPS

Experimental Setup and Methodology

The possibility of remote analysis was investigated by use of a telescopic focusing system and standard hardware. The experimental arrangement, shown in Figure 4-11, included the same 50 mJ Nd:YAG laser (Big Sky Laser Technologies, Inc.) which was used in the other experiments, a telescopic focusing system, a large diameter collection lens, and the fiber optic mini spectrometer (Ocean Optics, Inc.). The laser spark was

induced on a solid target placed at a distance of 6 m from the laser operating at its fundamental wavelength of 1064 nm at a maximum repetition rate of 20 Hz. The laser light was focused on the target by a telescopic beam compressor with an adjustable focal length. Emission from the spark was collected by a large quartz lens (10 cm diameter, 20 cm focal length) at a small angle with respect to the laser beam. The lens focused the plasma emission light on the face of an optical fiber (600 μm) and the fiber guided the light into the spectrometer. The two channel spectrometer alternatively covered the spectral ranges of 230-310 nm and 200-850 nm with resolutions of 0.5 nm and 1 nm, respectively.

Results

Typical spectra obtained with the remote LIPS system are shown in Figure 4-12. The spectra from the low-resolution channel (200-850 nm spectral range), Figure 4-12(b), are twice as intense as the spectrum from the high-resolution channel (230-310 nm spectral range), Figure 4-12 (a), due to the higher spectrometer sensitivity in the wide spectral range. Nevertheless, strong lines of elements could clearly be seen and resolved in both channels. Figure 4-13 shows a dramatic decrease in the line intensity ratio as the target distance was increased.

Overall, it has been demonstrated that a compact and reliable moderate power laser (the 50 mJ Big Sky) together with a simple and inexpensive detection system (the Ocean Optics spectrometer) can efficiently be used for remote detection of elements in solid samples within an operating distance of ~10 ft. The small size of the setup components is an additional advantage that allows the engineering of a compact setup for field applications.

The Portable LIPS Probe

Experimental Setup and Methodology

A schematic and picture of the portable LIPS probe are shown in Figures 4-14 and 4-15. Including the handle, the unit is 3 feet tall, allowing for convenient measurements at ground level by a standing operator. The operator grasps the handle of the unit at waist level and initiates the laser pulse by the trigger button on the handle. The trigger button, on/off switch, and safety interlock switch, are connected in series to initiate the laser trigger. The safety interlock switch is a precautionary device, allowing the laser to trigger only if the unit is pressed against a firm surface. This trigger circuitry is then connected by a 20 ft coaxial cable to the laser trigger box (Figure 4-10) on the back of the laser ICE (integrated cooler and electronics). The trigger circuit serves as the external trigger for the initiation of each laser pulse.

The customized unit is constructed within an aluminum frame. Laser light emitted from the laser head is focused by a lens at a fixed distance at the bottom of the probe. Light emitted from the plasma is collected by a pierced mirror and focused into an optical fiber. The 15 inch optical fiber is attached to a USB2000 Ocean Optics spectrometer. The spectrometer and notebook computer are linked by a short USB cable.

The software was customized for this application in Visual Basic 6.0 to allow for rapid identification of materials as overburden, matrix, or bedrock. "Training" of the software is done by constructing a spectral library of known materials. The spectra of unidentified samples are then correlated against the reference library. With each laser pulse, the software identifies the material as overburden, matrix, or bedrock, based on the magnitude of the correlation coefficient. A lightweight, Sony VAIO notebook computer was attached to the portable instrument for data acquisition and display.

Wet vs. Dry sampling

The effect of moisture on the spectroscopic behavior of real samples was investigated. The moisture content of the samples was determined by weight loss after drying. Spectroscopic data were taken on both wet and dry samples. The spectra of wet vs. dry samples were compared and the accuracy of identification was evaluated.

Real Sample Analysis

Several spectra were taken of overburden, matrix, and bedrock samples provided by IMC-Agrico. Samples were studied as received and had varying, unknown moisture content. Three samples of each material were used.

Ten spectral libraries were made from these nine samples, each library consisting of the data points from each spectrum of overburden, matrix, or bedrock. Correlation coefficients were obtained for each sample with respect to other samples within the same library. These correlation coefficients from the 10 libraries were averaged and the standard deviation was calculated.

IMC-Agrico Site Visit

At the New Wales facility, a number of samples were taken directly from the mining facility and analyzed by LIPS. The portable LIPS probe was first used on a variety of samples on hand. Samples were placed in a 13 x 9 inch pan for the analysis by the probe. Here, an identification of each of the 11 samples was determined after 20 single shots of the probe. The following day, the probe was taken outdoors for analysis directly on mounds of material that a nearby dragline had recently unearthed. A generator placed in the bed of the truck supplied power. Finally, a number of samples were obtained from various mine pits and were sent to the University of Florida for LIPS analysis.

Results

Samples obtained directly from IMC-Agrico are typically moist. Moisture content as received is at most 20%. Average moisture content for matrix and bedrock samples is 16% and for overburden less than 2%. Correspondingly, samples of overburden are less affected by moisture since the typical real sample does not contain as much moisture as that of matrix and bedrock samples. The intensity of the signal from overburden is reduced by approximately 15-20%, while the reduction in signal intensity of the more moist samples of matrix and bedrock is typically 30-60% (Figures 4-16 to 4-18).

The reduction in signal intensity when dealing with real samples, however, does not influence the software's ability to accurately identify the samples. Each spectrum is rich with spectral information, provided a good laser shot is taken. The training set in the library accounts for the moisture in the samples, resulting in accurate identification with each laser trial. Thus, a comprehensive library will yield more accurate identification. Because of the distinct differences among the three types of samples, the effect of moisture has little effect on the accuracy of identification.

The averaged correlation coefficients from real sample analysis are displayed in Table 4-6. Again, as has been shown previously in preliminary results and in the benchtop design, the software easily distinguishes among overburden (O1, O2, O3), matrix (M1, M2, M3), and bedrock (B1, B2, B3) with this LIPS probe design. The correlation coefficients for the samples are graphically displayed in Figures 4-19 to 4-21. Correlation coefficients of each layer are high within each group, indicating a high accuracy in classifying the soils. The average standard deviation is 0.108, indicative of a high precision from these unprepared samples. There are some occasions in which the

correlation coefficients of a sample do not correlate well with others of the same classification (M1 and B2). Practically, this inaccuracy would easily be resolved as successive determinations are expected to be made on samples of the same classification. It is observed, however, that this instrument and software provide a very reliable identification of material as overburden, matrix, or bedrock.

At the New Wales facility, the results from the first day of analysis were positive. Of the 11 samples, 8 were identified correctly according to the chemical analysis. Positive identification was established as the material identified in majority relative to the other two possibilities. Typically, this was achieved by about 16 of the 20 laser shots identifying a particular material.

Results from the outdoor analysis near the mine pit were similar. Issues regarding the application of the instrument to the field became apparent. The most obvious was the visibility of the computer monitor in bright sunlight. Reflection of the sun on the computer monitor made the operation of the instrument cumbersome and difficult. In addition, the sampling of materials was also laborious. The coolant and power cables for the unit allowed only a 20 ft measuring range, which was found to be inconveniently short. Thus, visible mounds of material just several yards away needed to be brought to the unit for analysis. Despite these rather simple problems, the field performance of the probe was encouraging overall, noting the ruggedness of the instrument and the accuracy of the identification.

The results from the analysis of the samples that were sent to the University of Florida for LIPS analysis are included in Table 4-7. The LIPS method was accurate with 9 of the 15 samples, assuming the chemical analysis is accurate. However, an

interpretation of the chemical analyses provides insight into the errant samples. For example, lab analysis of sample 1 indicates a high content of bone phosphate lime (BPL) and a marginal (but high) MgO. Officially, the geology department cuts off the ore body at MgO of 0.8%. In the chemical classification algorithm used, 2% MgO was used as a cutoff because the tendency is to blend away the higher MgO product. At the particular location where this sample was mined (Hopewell), the MgO increases more gradually so that the ore contact is not sharply defined. Thus, the sample is marginally bedrock, but is likely in the lower contact transition region. Sample 1 could be classified as either matrix or bedrock. It was classified as matrix by the chemical analysis and bedrock by the LIPS analysis.

Sample 5 was classified as overburden by chemical analysis and as matrix by LIPS analysis. A visual analysis of the material indicates that the sample is clearly overburden. This was likely a case in which the spectral library used is not as comprehensive as possible. If more representative spectra were included in the library, perhaps this sample would have been identified correctly.

Sample 10 was taken from the center of the ore body in what was believed to be a barren strip of clay. Chemical analysis reveals it to be overburden, while LIPS analysis identifies it as matrix. The sample does have lower BPL levels than desirable (9.78%), but the marginal MgO content indicates that the sample is probably adequate for mining. Sample 13 behaves similarly. The MgO level is low, while the BPL content (9.06%) is slightly lower than the cutoff value desired (10%). These are good examples of samples in which the analyses using LIPS might be more reliable than those obtained from conventional chemical analyses.

Finally, with these interpretations in mind, the LIPS algorithm appears to give an accurate, or at least reasonable, identification with 13 of the 15 samples that were sent to the University for analysis. The identification of the 2 incorrect samples may be due, in large part, to the exclusiveness of the present spectral library.

Conclusions

One immediate application of the remote probe could be the analysis of raw ores at industrial beneficiary sites. No sample preparation is required and a quick identification of the nature of a material can be obtained.

Although the fiber optic probe was functional, it was difficult to obtain sufficient laser irradiance at the sample, after re-collimating and re-focusing the output of the fiber optic link. With the irradiance obtained, it was difficult to obtain a reproducible, energetic plasma on some soils, especially if the sample was wet. The study was therefore completed using a system that incorporated the laser head within the measurement probe.

The benchtop laboratory instrument was used as a prototype for preliminary study before the development of the field LIPS probe. Similar studies were performed on both instruments to assess the accuracy of sample identification with real samples. The field LIPS probe is engineered for robust use on site and provides a rapid identification of material using the software developed.

The studies presented here have given encouraging results. Specifically, the soils were easily identified as overburden, matrix, or bedrock using a single shot spectrum. In summary, we have

- shown that overburden, matrix, and bedrock can be easily distinguished;

- demonstrated remote identification at a range of 10 m;
- developed a field LIPS probe for single shot material identification; and
- developed software that displays correlation results with each laser pulse.

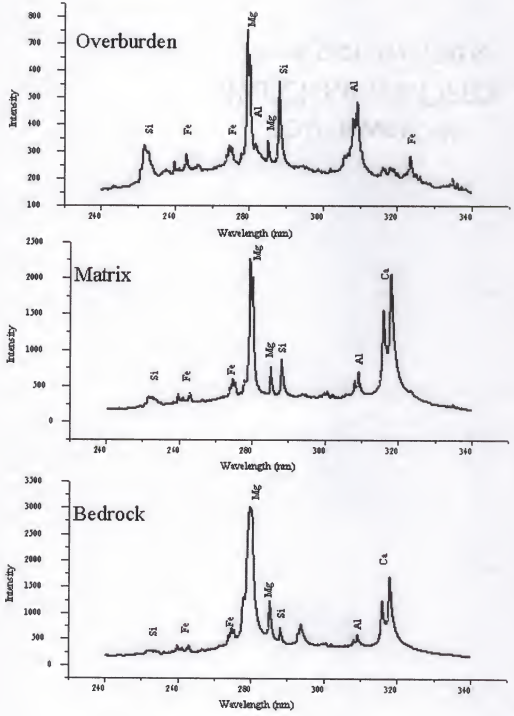

Figure 4-1. LIPS spectra of overburden, matrix, and bedrock.

Table 4-1. Average spectral line intensity ratios.

Sample	Si/P	Si/Mg	Si/Al	Si/Fe
A1	169 ± 91	11 ± 6	16 ± 5.5	10.4 ± 6.4
A2	48 ± 30	2.4 ± 0.4	15 ± 4.3	3.3 ± 0.9
A3	39 ± 22	0.33 ± 0.07	17 ± 7.7	2.2 ± 0.7
B1	89 ± 42	17.3 ± 8	10.4 ± 3.3	12.8 ± 3.7
B2	118 ± 55	2.0 ± 0.4	16.7 ± 4	2.2 ± 0.4
B3	118 ± 40	0.53 ± 0.2	27.3 ± 9	1.86 ± 0.3

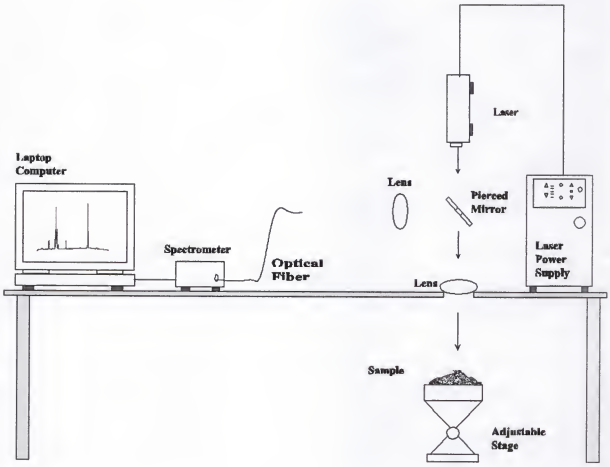

Figure 4-2. Schematic of the LIPS benchtop experimental system.

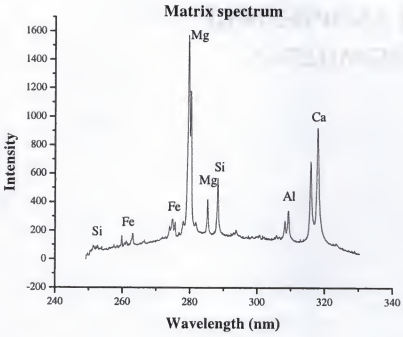

Figure 4-3. LIPS emission spectrum of matrix sample.

Table 4-2. Correlation coefficients for overburden, matrix, and bedrock samples.

Sample	O'burden 1	O'burden 2	Matrix 1	Matrix 2	Bedrock 1	Bedrock 2
O'burden 1	1	0.9568	0.5756	0.7026	0.5056	0.4424
O'burden 2	0.9568	1	0.5617	0.6599	0.4503	0.3753
Matrix 1	0.5756	0.5617	1	0.9289	0.7639	0.7106
Matrix 2	0.7026	0.6599	0.9289	1	0.8184	0.7674
Bedrock 1	0.5056	0.4503	0.7639	0.8184	1	0.9785
Bedrock 2	0.4424	0.3753	0.7106	0.7674	0.9785	1

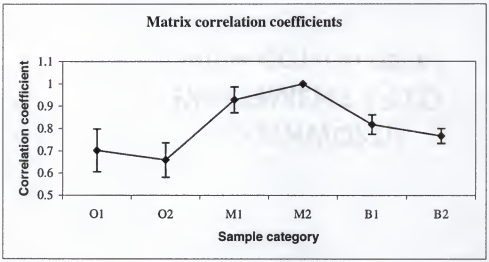

Figure 4-4. Correlation coefficients of matrix sample.

Table 4-3. Identification of materials by chemical and LIPS analysis.

Sample	$\%P_2O_5$	%MgO	Chemical ID	LIPS ID
1	7.31	6.02	Bedrock	Bedrock
2	3.03	6.72	Bedrock	Bedrock
3	3.62	1.67	Matrix/Bedrock	Bedrock
4	1.12	15.03	Bedrock	Matrix
5	4.80	3.81	Bedrock/Matrix	Bedrock
6	ND	0.22	Overburden	Overburden
7	16.19	0.21	Matrix	Matrix
8	2.95	6.14	Bedrock	Bedrock

Table 4-4. Criteria for classification by chemical analysis.

	P_2O_5	MgO
Overburden	Negligible	Negligible
Matrix	≥ 3%	≤ 1.5 %
Bedrock	Variable	≥ 5%
Anything in between is a mixture.		

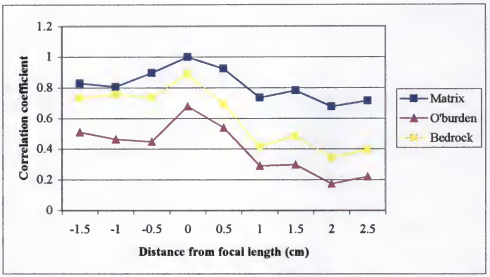

Figure 4-5. Correlation coefficients as a function of distance from focal length at maximum laser power.

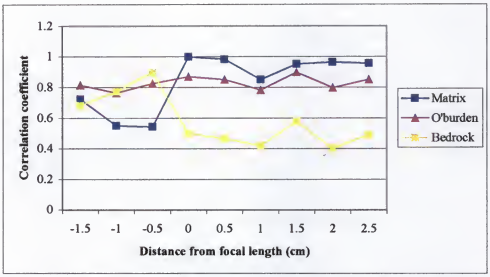

Figure 4-6. Correlation coefficients as a function of distance from focal length at lower laser power.

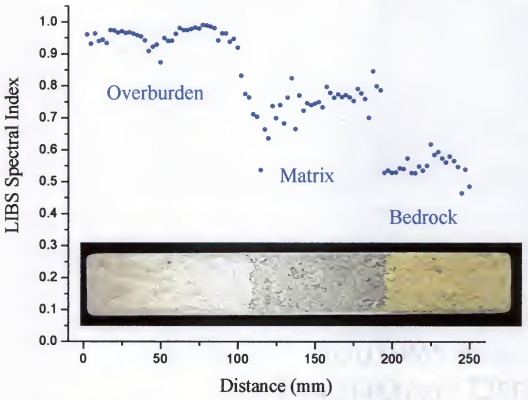

Figure 4-7. Plot of correlation coefficients vs. distance using motorized sample translation.

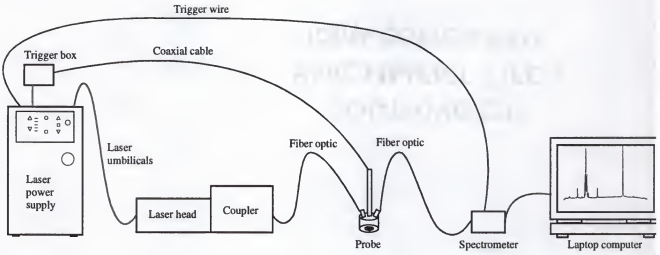

Figure 4-8. Fiber-optic probe system.

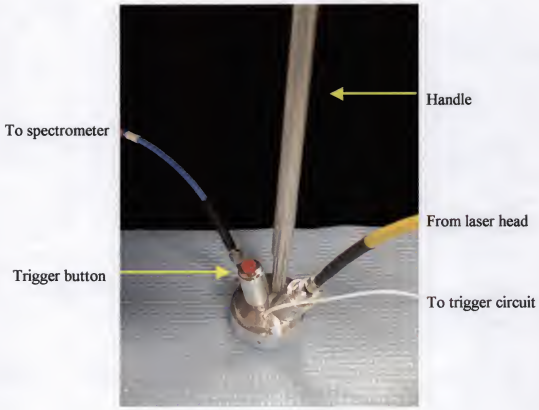

Figure 4-9. Fiber optic LIPS probe.

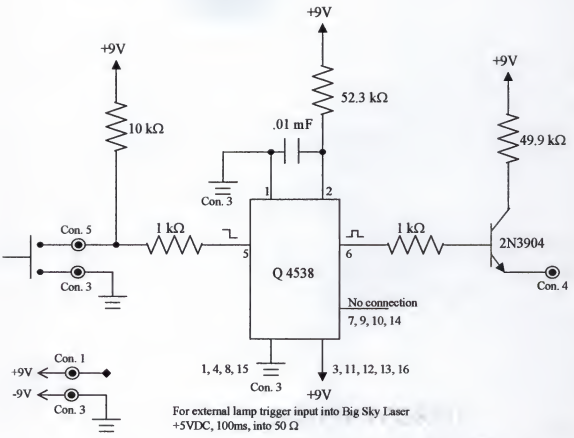

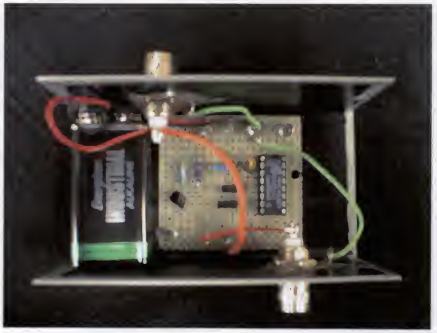

Figure 4-10. Trigger circuit for Big Sky laser.

Table 4-5. Identification using a fiber optic LIPS probe.

	Overburden	Matrix	Bedrock
Correct	174	159	188
Incorrect	4	10	11
Poor spectra (Corr. Coeff. < 0.5)	22	31	1

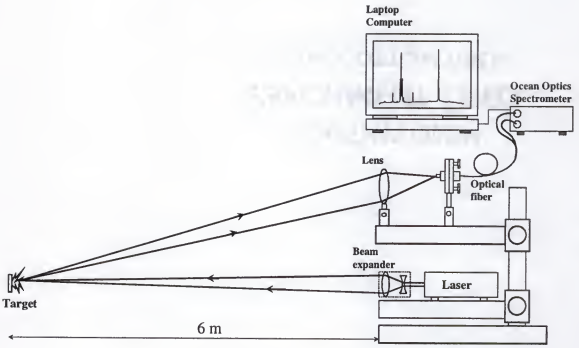

Figure 4-11. Experimental apparatus for remote LIPS.

(a) Spectra obtained with LIP-spectrometer at the distance of 6 m using low- and high resolution spectrometer channels

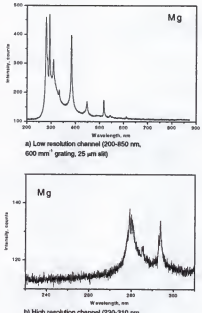

(b) Spectra obtained with LIP-spectrometer at the distance of 6 m

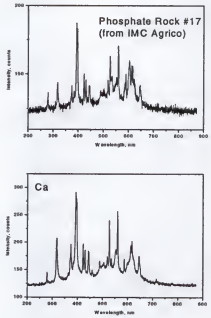

Figure 4-12. Remote LIPS spectra.

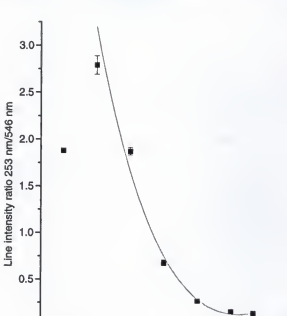

Figure 4-13. Line intensity ratio as a function of distance in remote LIPS analysis.

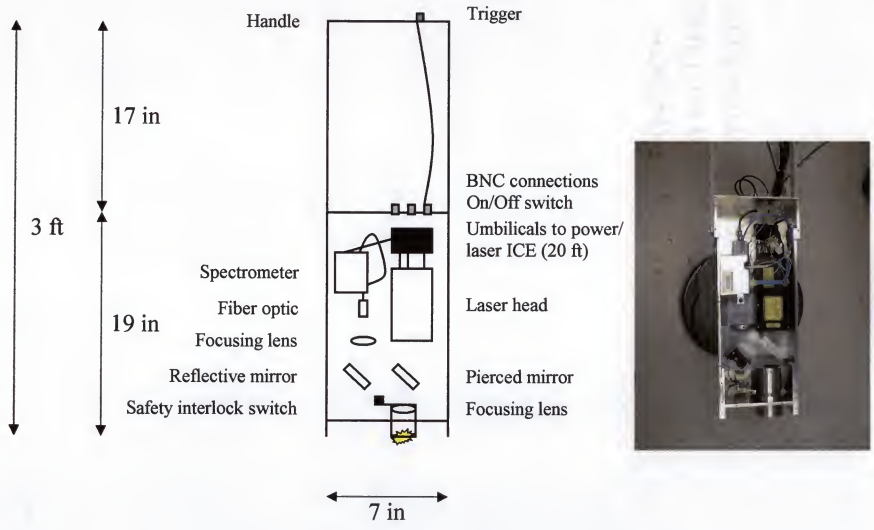

Figure 4-14. Experimental setup of the field LIPS probe.

Figure 4-15. The field LIPS probe.

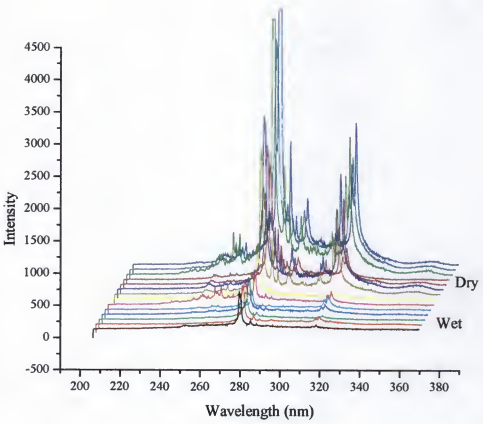

Figure 4-16. Spectra of wet and dry bedrock samples.

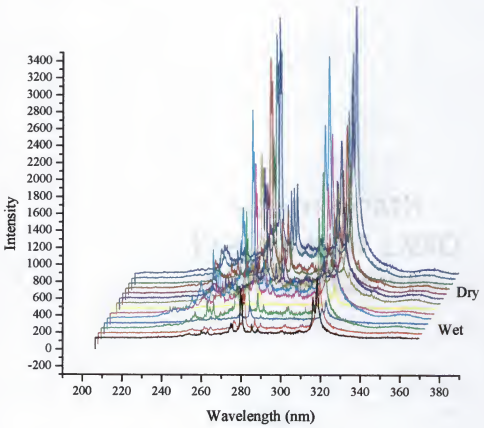

Figure 4-17. Spectra of wet and dry matrix samples.

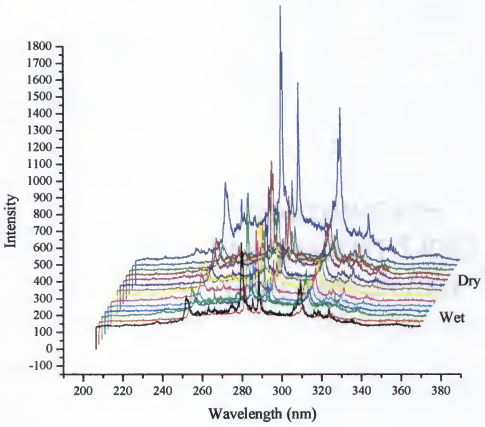

Figure 4-18. Spectra of wet and dry overburden samples.

Table 4-6. Correlation coefficients for overburden, matrix, and bedrock untreated samples.

	O1	*O2*	*O3*	*M1*	*M2*	*M3*	*B1*	*B2*	*B3*
O1	1	0.9009	0.9010	0.6916	0.5490	0.6382	0.6624	0.8346	0.7453
O2	0.9009	1	0.9167	0.7237	0.6580	0.6996	0.6189	0.8216	0.7366
O3	0.9010	0.9167	1	0.7651	0.6311	0.6348	0.6644	0.8391	0.7534
M1	0.6916	0.7237	0.7651	1	0.7548	0.7284	0.7360	0.7603	0.7543
M2	0.5490	0.6580	0.6311	0.7548	1	0.7846	0.6057	0.5563	0.5994
M3	0.6382	0.6996	0.6348	0.7284	0.7846	1	0.6506	0.6539	0.6874
B1	0.6624	0.6189	0.6644	0.7360	0.6057	0.6506	1	0.7718	0.8524
B2	0.8346	0.8216	0.8391	0.7603	0.5563	0.6539	0.7718	1	0.8387
B3	0.7453	0.7366	0.7534	0.7543	0.5994	0.6874	0.8524	0.8387	1

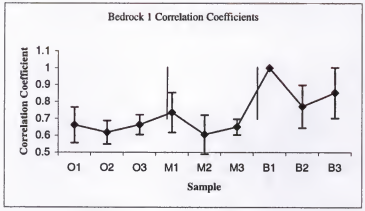

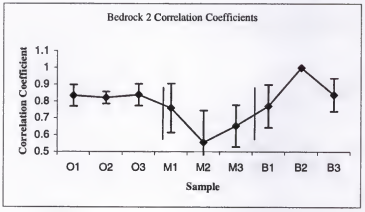

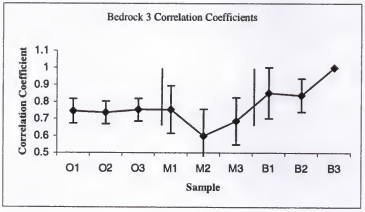

Figure 4-19. Bedrock correlation coefficients.

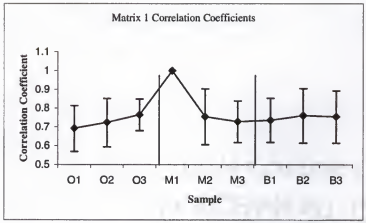

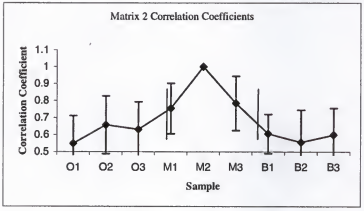

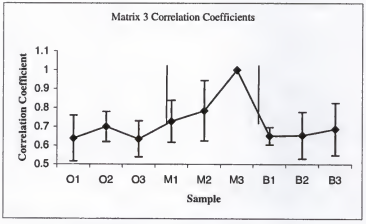

Figure 4-20. Matrix correlation coefficients.

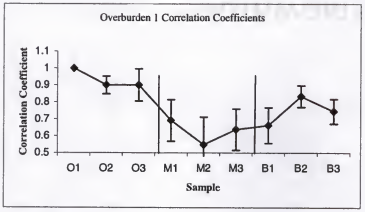

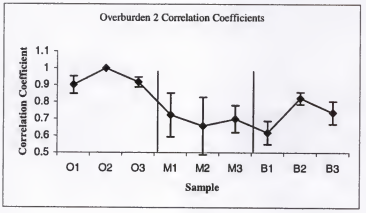

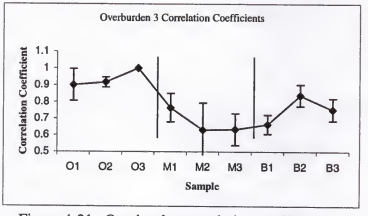

Figure 4-21. Overburden correlation coefficients.

Table 4-7. Chemical and LIPS analysis results from IMC-Agrico samples.

	BPL	Fe_2O_3	Al_2O_3	Insol.	CaO	MgO	Chemical Analysis ID	LIPS ID	
1	21.25	2.47	1.93	61.9	13.95	1.6	Matrix	Bedrock	x
2	4.31	0.22	2.46	89.45	0.47	0.06	Overburden	Overburden	ok
3	29.29	0.74	2.34	56.49	18.3	0.39	Matrix	Matrix	ok
4	14.38	1.8	0.68	8.18	30.44	14.59	Bedrock	Bedrock	ok
5	0.26	0.2	0.08	95.05	0.21	0.03	Overburden	Matrix	x
6	43.57	0.41	3.8	41.49	24.77	0.08	Matrix	Overburden	x
7	7.18	0.68	0.59	26.16	24.11	12.38	Bedrock	Bedrock	ok
8	21.65	0.47	4.74	67.58	5.11	0.21	Matrix	Matrix	ok
9	19.71	0.77	1.3	69.27	12.58	0.38	Matrix	Matrix	ok
10	9.78	1.96	3.28	73.78	6.49	0.82	Overburden	Matrix	x
11	4.07	0.53	0.66	15.61	26.02	16.08	Bedrock	Bedrock	ok
12	16.14	0.59	1.54	74.84	9.73	0.22	Matrix	Matrix	ok
13	9.06	0.43	1.72	82.82	3.55	0.03	Overburden	Matrix	x
14	0.69	0.31	1.37	89.68	0.19	0.02	Overburden	Overburden	ok
15	12.01	0.95	1.38	75.56	8.68	0.69	Matrix	Bedrock	x

CHAPTER 5
LIPS FOR CHARACTERIZATION OF ARCHAEOLOGICAL MATERIALS

Introduction

In recent years, there has been increasing use of modern laser technology in archaeology, and the results are particularly promising. One of the principal tasks of excavation teams is the establishment of a meaningful classification of the many recovered ceramic materials. A number of techniques, involving visual examination as well as mineralogical, chemical, structural, and elemental analysis, has been used in characterizing and subsequently classifying ceramic materials [24]. Micromorphological comparison of pottery groups and soil materials has indicated that two main factors influence the raw material procurement strategies of the potters of these settlements: the proximity of the soil material to the potter's settlement and the suitability of the soil material for pottery manufacture. Wieder and Adan-Bayewitz studied different pottery groups from the Roman period [25]. Several techniques have been proposed as tools for archaeological analysis. Clark and Gibbs examined the pigments of a number of pieces by Raman microscopy using an Olympus BH-2 microscope with a 100x objective coupled to a DILOR X-Y triple grating spectrometer with a photodiode-array detector [26]. The light sources were either a Coherent 170 argon ion laser or a krypton ion laser. An extensive evaluation of common pottery from Roman Galilee and Golan was carried out, employing neutron activation analysis to determine the primary classification of archaeological materials [27]. Characterization of archaeological material was performed using Mossbauer spectroscopy [28], and non-destructive x-ray fluorescence (XRF) has

been used by several workers for the analysis of archaeological materials [29, 30]. Thermogravimetry (TG) and differential thermal analysis (DTA) were used by Papargyris and Cooke for ceramic powders [31]. X-ray diffraction (XRD) and scanning electron microscopy (SEM) analyses have been used to obtain fractionated particle sizes of dolomite [32].

LIPS has been used to identify metallic elements in vitrified glass [33] and pigments used in painting [34]. Analysis of pigments in paintings is of major significance in art conservation, as it can lead to detailed characterization of materials as discussed in Chapter 2. Thus, pigment analysis is important for dating and authentication as well as for possible conservation of restoration of the artwork. Burgio et al. used two laser-based analytical techniques—LIPS and Raman microscopy [35].

The LIPS technique has been successfully applied as an on-line diagnostic technique in the laser cleaning process of polluted limestone from historic buildings of the Spanish Renaissance [36]. The classification of pottery by laboratory analysis depends upon matching the composition of the pottery. The criteria for selecting reference pottery depend upon the archaeological problems and will not be discussed here. The analyzed materials have homogeneous compositions and are not grossly different in composition. The geographical domain for the present study was confined to Spain. The key Spanish city of Zaragoza was an important center for pottery manufacture during the Roman period. Over 2,000 years of history have left Zaragoza with a series of cultural strata that have gradually formed the personality and physiognomy of a large, modern city which, at the same time, has its roots firmly planted in its past.

In previous papers [20, 37], it has been shown that simple statistical correlation methods, such as linear and rank correlations, can be successfully applied for identification of solid and particulate materials using laser-induced plasma spectroscopy. A compact LIP spectrometer with microscopic sample imaging was used for rapid identification of plastics [38]. Emission spectra were collected with a compact, dual channel, fiber optic spectrometer and monitored either in a 230-310 nm or a 200-800 nm spectral window. Linear and nonparametric rank correlation methods were used for identification of plastic samples which had very similar compositions. A nearly 100% reliable identification was achieved. In another study, identification of particulate materials, such as iron ores and iron oxides, also yielded nearly 100 % accuracy [38]. The success of the correlation approach is based on the use of thousands of data points (pixels) representing the sample spectrum in a relatively large spectral window.

In this chapter, the application of linear and nonparametric rank correlation for the identification of various pottery types is demonstrated.

Experimental

Instrumentation

Micro-LIPS system

A microscopic LIP spectrometer, developed in the laboratory, has been previously described [20]. Briefly, it consists of a compact Nd:YAG laser (model MK-367) which is attached to a modified microscope. The laser output is aligned with the microscope optical system using a dichroic mirror placed inside the microscope enclosure. The mirror reflects 99% of the laser radiation at 1064 nm and transmits visible light coming from the illuminated sample. A magnified image of the sample is monitored with a TV camera mounted on the top of the microscope and connected to a monitor. Microscope

magnification is varied with a set of objectives placed in a rotatable mount. For the present work, a 10x objective (total magnification 500x) is used with a working distance of 5 mm between the objective tip and the sample surface. With the 10x working objective, the laser is focused to a ~ 20 μm diameter spot on the sample surface providing an irradiance of ~ 10^{12} W/cm^2. The laser and the spectrometer are synchronized by a trigger pulse from a home-made compact pulse generator working either in a single pulse mode or at a 0.5 Hz repetition rate.

Mini-LIPS system

The mini-LIPS system consists of a compact Nd:YAG laser. The mirror reflects 99% of the laser radiation at 1064 nm and transmits visible light coming from the illuminated sample. The laser and the spectrometer were synchronized by a trigger pulse from a custom-built compact pulse generator working either in a single pulse mode or at a 0.5 Hz repetition rate.

In both cases the radiation from the laser spark was collected with a bifurcated optical fiber connected to a dual-channel Ocean Optics mini-spectrometer (SD2000). The spectrometer had the following characteristics: channel one—230-310 nm spectral range, 3600 mm^{-1} holographic grating, 25 μm slit, 0.16 nm spectral resolution, 2048 pixel linear CCD array; channel two—200-850 nm spectral range, 600 mm^{-1} grating blazed at 400 nm, 25 μm slit, 1.3 nm spectral resolution, 2048 pixel linear CCD array. The spectrometer was driven from a laptop computer *via* a DAQCard-700 interface (National Instruments). Data acquisition and analysis were performed using software (Visual Basic 6.0) written in-house.

Samples

The first six samples examined were generously obtained form Department of Ancient Sciences of the University of Zaragoza and the majority were collected by excavations at Zaragoza, Spain. The city of Zaragoza, founded by Augustus Caesar, is very important for archaeology as it contains the remains of a Roman city established two thousand years ago. Descriptions of the sample fragments are given in Table 5-1. Samples 1-6 are from Spain and samples 7 and 8 are ceramics from Italy.

LIPS Libraries

LIPS libraries were compiled for identification of the ceramic materials. The library spectra were obtained by inducing the laser spark on 10 random surface spots and averaging the resulting 10 emission spectra. All libraries were stored in a computer and used on a day-to-day basis without being renewed.

Software

A program for correlation analysis was developed using Visual Basic 6.0 and the LabView drivers supplied with the Ocean Optics spectrometer. A detailed description of the program can be found elsewhere [20]. In brief, the software offered the following options to an operator: (i) choice of appropriate experimental parameters (integration time, trigger type, spectrometer channel, number of spectra to average, library file); (ii) pre-treatment of the spectrum (reduction in the spectral range, correction for continuous plasma background); and (iii) selection of a correlation method (linear or rank). The computer calculated all mutual correlation coefficients between the current spectrum and all library spectra. The correlation plot corresponding to the maximum correlation coefficient was displayed along with the statistical parameters (correlation coefficients, errors, probabilities) and the name of the compound which is identified with the highest

correlation probability. If desired, the correlation can be repeated with the use of another correlation method. The output data are saved and stored in a computer.

Results and Discussion

Small amounts of materials (micrograms) like ceramics are almost entirely atomized when exposed to laser radiation sufficient intense for breakdown. The application of LIPS for identification of materials is especially good because there is no loss of information in the plasma. As shown in these results, the large amount of spectroscopic data (2,048 pixels), used in the correlation procedure, allowed original information about the sample nature to be obtained.

The correlation methodology was first applied to library ceramics S1 through S6 using the micro-LIPS system. Ten shot-averaged spectra from these samples are shown in Figure 5-1. The most prominent feature in all the spectra is an unresolved group of N II lines near 500 nm due to atmospheric nitrogen. A group of O II lines also appear in the region 350-450 nm and the O I triplet at 777.2-777.5 nm is also visible. Other features include a strong carbon line at 247.86 nm and the H_α line at 656.28 nm. Visual examination of Figure 5-1 does not reveal any obvious differences in the spectra. However, one would only expect subtle variations in the ratios of line intensities, due to the varying stoichiometry of the various ceramics and also small variations in the nature of the background spectra due to differences in the laser material interaction. These subtle, yet consistent, differences in the spectra can be reliably discerned using a simple linear or rank correlation analysis [20].

Eight materials were chosen as indicated in Table 5-1. The results of identification using 10 shot-averaged spectra are shown in Tables 5-2 and 5-3. Both correlations show very high (>90%) probabilities of correct identification, except for a

few cases. There is some potential for improvement in the robustness of this technique. Additional software options can be applied in order to increase the probability of correct identification. For example, spectra pre-treatment options can be used which include choice of spectral range. Increasing the spectral range may be useful when a large portion of the recorded spectrum contains no information, or only spectral features which are related to the sample composition. Elimination of the uninformative portion of the spectrum may improve correlation results.

In our case, the central portion of the spectrum (containing the strong group of N II lines) was entirely due to the surrounding air and not from the pottery. Therefore, it was logical to exclude this portion from the correlation analysis. The probability of identification was somewhat improved in the case of linear correlation and rank correlation (see Table 5-3).

Obviously, any spectral information relating to the O and N content of the ceramics was lost in our measurements because the spectra were taken in air. Although the reliability of identification might be significantly improved if the samples were studied in an inert environment, this was not done because of the interest in the development of an approach that would be useful for rapid identification of ceramics in a normal environment.

The other options for improvement of the robustness are instrumental. As shown previously [20], higher spectrometer resolution results in an increased probability of correct identification. Similarly, a wider spectral range is useful if it is not obtained at the expense of resolution. Ideally, high resolution and wide spectral range, combined

together (as in an echelle spectrometer) would provide the best possible performance for the proposed correlation routine, but at a significant increase in cost.

Summary and Conclusions

Pottery groups manufactured in ancient settlements of early Roman (late first century BC) were studied by LIPS. The goal of this work was the instant identification of ceramics by LIPS. LIP spectra from ceramics in a 200-800 nm spectral window were compared with reference spectral libraries stored in a computer. The libraries consisted of representative spectra from different groups of ceramic samples. The plasma emission spectra of eight archaeological samples were studied. Simple statistical correlation methods including linear and rank correlations were used. The probabilities of correct identification ranged from 0.8 to 1 with values close to unity for most of the samples studied. The present study aids in the characterization and identification of different types of materials used in pottery by means of LIPS, which is essentially non-destructive to the ceramic.

A compact laser-induced plasma spectrometer has been used for rapid classification of different groups of old ceramics by using statistical correlation analysis. A customized software package was implemented which combined both data acquisition and data processing functions. Linear and non-parametric (rank) correlations were applied for classification of spectral data with approximately the same results. The robustness of the technique was demonstrated by achieving 90-99% reliable identification of almost all analyzed ceramics. The technique has excellent potential for on-line, real-time analysis of archaeological materials.

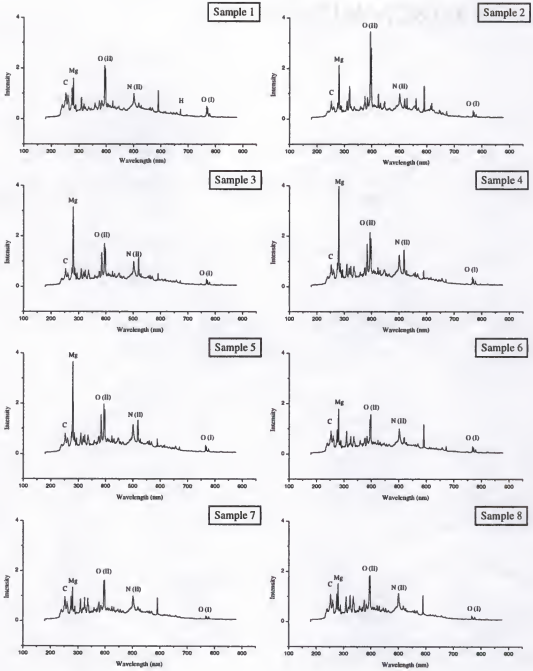

Figure 5-1. LIP spectra from archaeological ceramic samples.

Table 5-1. Description of pottery samples.

Sample	Material	Origin	Description
S1	Labitolosa. Terra Sigilata Hispanica	Villaroya de la Sierra (Zaragoza), Spain	Concave fragment, orange with a design length, 4.0 cm; width 4.0 cm.
S2	Labitolosa. Terra Sigilata Hispanica	Tricio (La Rioja), Spain	Orange, curved fragment; length, 4.5 cm; width, 2.0 cm.
S3	Labitolosa. Typical oxidant ceramic	Zaragoza, Spain	Orange, curved fragment: length, 5.5 cm; width, 4.0 cm.
S4	Labitolosa. Typical reducing ceramic	Zaragoza, Spain	Black, curved fragment: length, 5.0 cm; width, 3.5 cm.
S5	Lumpy ceramic	Zaragoza, Spain	Orange, curved fragment; length, 6.0 cm; width, 4.5 cm.
S6	Typical ceramic	Botorrita (Zaragoza), Spain	White, curved fragment; length, 4.5 cm; width, 4.0 cm.
S7	Recent pottery	Italy	Red, curved fragment; length, 6.5 cm; width, 5.5 cm.
S8	Recent pottery	Italy	Red, curved fragment; length, 8.0 cm; width, 6.5 cm.

Table 5-2. Calculated probabilities in ceramic archaeological samples using the mini-LIPS system from 230-315 nm.

	Linear correlation (Rank correlation)							
Samples	S1	S2	S3	S4	S5	S6	S7	S8
S1	0	1	0.5069	0.9961	0.9434	1	0.9155	0.9033
	(0)	(0.0730)	(0.2011)	(0.9983)	(0.9526)	(1)	(0.9976)	(0.9992)
S2	0.9467	0	0.4654	1	0.9490	1	1	1
	(0.0924)	(0)	(0.4859)	(1)	(0.9839)	(1)	(1)	(1)
S3	1	1	0	1	1	1	1	1
	(0.9453)	(0.9933)	(0)	(0.9991)	(0.5088)	(1)	(1)	(1)
S4	0.9769	0.9953	0.9329	0	0.9999	1	0.9985	0.9854
	(0.5454)	(0.2963)	(0.5088)	(0)	(0.9998)	(1)	(0.9986)	(0.9897)
S5	0.9910	1	1	1	0	0.0970	0.9887	0.9701
	(0.7704)	(0.9857)	(0.8340)	(0.9991)	(0)	(0.8886)	(1)	(1)
S6	1	1	1	1	1	0	1	1
	(1)	(1)	(1)	(1)	(1)	(0)	(1)	(1)
S7	0.9985	0.9994	0.9999	1	0.9105	1	0	0.9951
	(0.9563)	(0.9986)	(0.9097)	(0.9416)	(0.9081)	(1)	(0)	(0.2565)
S8	0.9947	1	0.8393	0.9816	1	1	1	0
	(0.9987)	(0.3542)	(0.9711)	(0.8993)	(0.9768)	(1)	(0.9140)	(0)

Table 5-3. Calculated probabilities in ceramic archaeological samples using the micro-LIPS system from 180-315 nm.

	Linear correlation (Rank correlation)							
Samples	S1	S2	S3	S4	S5	S6	S7	S8
S1	0 (0)	1 (1)	1 (1)	1 (1)	1 (1)	1 (1)	1 (1)	1 (1)
S2	0.9999 (0.9988)	0 (0)	1 (1)	1 (1)	1 (1)	1 (1)	1 (1)	0.9812 (0.9999)
S3	1 (1)	1 (1)	0 (0)	1 (1)	1 (1)	1 (1)	1 (1)	1 (1)
S4	1 (1)	1 (1)	1 (1)	0 (0)	1 (1)	1 (1)	1 (1)	1 (1)
S5	1 (1)	1 (0.9999)	1 (1)	1 (1)	0 (0)	1 (1)	1 (1)	0.9999 (0.9991)
S6	1 (1)	0.9989 (1)	1 (1)	1 (1)	0.9977 (0.9985)	0 (0)	0.9999 (0.9996)	0.9790 (0.9984)
S7	1 (1)	1 (1)	1 (1)	1 (1)	1 (1)	1 (1)	0 (0)	1 (1)
S8	1 (1)	0.9989 (0.9963)	1 (1)	1 (1)	1 (0.9999)	0.9999 (0.9998)	1 (1)	0 (0)

CHAPTER 6
ANALYTICAL MATRIX EFFECTS IN GEOLOGICAL MATERIALS

A microscopic laser-induced plasma spectrometer was used to evaluate the analytical matrix effect commonly observed in the analysis of geological materials. Samples were analyzed in either the powder or pressed pellet forms. Calibration curves of a number of iron and aluminum compounds show a linear relationship between the elemental concentration and peak intensity. A direct determination of elemental content can thus be made from extrapolation on these calibration curves. To investigate matrix effects, synthetic model samples were prepared from various iron and aluminum compounds spiked with SiO_2 and $CaCO_3$. The addition of these matrices had a pronounced analytical effect on those compounds prepared as pressed pellets. However, results indicated the absence of matrix effects when the samples were presented to the laser pulse as loose powders on adhesive tape. Results are comparable to certified values, indicating the reliability of this sampling approach for accurate analysis, provided the sample particle diameters are greater than ≈ 100 μm. Finally, the simultaneous analysis of two different elements was demonstrated using powders on tape.

Introduction

Laser-induced plasma spectroscopy is now a well-established technique for the elemental analysis of solid compounds. Although LIPS is advantageous in that it allows direct, rapid analysis with little or no sample preparation and is virtually non-destructive [39], LIPS signals emitted from the same element often depend on the matrix in which it is embedded [40].

Several groups have investigated analytical matrix effects in laser ablation. The dependence of matrix effects on plasma conditions was studied by measuring the ionic-to-atomic spectral line intensities of zinc and manganese following laser ablation into a dry inductively-coupled plasma (ICP) [41]. Others have also studied the effects of the matrix in laser ablation ICP mass spectrometry (LA-ICP-MS) and LA-ICP atomic emission spectroscopy (LA-ICP-AES) using geological materials prepared as pressed pellets [42, 43]. Chaléard et al. mathematically corrected for matrix effects by normalizing emission signals against the quantity of material vaporized and the plasma excitation temperature in LA optical emission spectrometry (LA-OES) [44]. Ciucci et al. incorporated a mathematical algorithm to overcome the analytical matrix effects [45]. Without the use of calibration curves, their method allowed precise and accurate determination of the elemental composition of materials using LIPS.

In this study, the analytical matrix effects of powdered samples using LIPS are compared to those observed for the same samples prepared as pressed pellets. The elemental composition of ores is determined by extrapolation from calibration graphs made from compounds with known elemental concentrations. This chapter also discusses the simultaneous quantitative analysis of the major constituents in ore powders using LIPS. To maximize the analytical performance of LIPS, a better understanding of these matrix effects is necessary.

Experimental

Apparatus

A compact LIP-spectrometer with microscopic sample imaging was used for quantitative spectrochemical analysis [20]. Spectra were collected with a compact dual channel fiber optic spectrometer and monitored either in a 230-310 nm or a 200-800 nm

spectral window. The instrumental configuration is the same as the micro-LIPS system described in Chapter 5.

Sample Preparation

To observe the effect of sample presentation in our system, samples having known concentrations of elements were prepared as either pressed pellets or powders. Each mixture was ground and homogenized for 30 minutes to ensure particle uniformity. For pressed samples, a portion of each mixture was transferred to an aluminum dish (32 mm diam., 7 mm deep) and compacted into a pellet with a force of 5000 kPa for 5 minutes. The powdered samples were placed on double-sided tape (3M) on a microscope slide. The powders were scattered over the tape surface ensuring that single particles, separated from each other by a distance of several particle diameters, could be distinctly seen.

Iron compounds [$Fe(NO_3)_3 \cdot 9H_2O$, $FeCl_2 \cdot 4H_2O$, Fe_3O_4, Fe] in the pressed and pellet forms were studied. Similarly, several aluminum compounds were analyzed. With the signal intensities of particular atomic lines (274.6 nm for Fe and 282.2 nm for Al) and the varied concentrations of iron and aluminum in these compounds, calibration graphs were prepared.

The matrices used were SiO_2 and $CaCO_3$ to represent the two important geochemical classes of silicates and carbonates. The various compounds of aluminum and iron were spiked with these matrices (at 70% matrix) to prepare calibration graphs. Matrix effects were investigated by examining the change in slope resulting from the addition of the matrix.

Other determinations were made to determine the accuracy of the technique, the effect of particle size, and the capability to simultaneously determine elemental content of different species in either the pressed or powdered form.

Results and Discussion

LIPS was used for several compounds of iron and aluminum using both powders and pellets. Calibration curves show a linear relationship between the concentration of the element and the peak intensity (Figure 6-1). The spectral lines used for compounds of iron and aluminum were 274 nm and 282 nm, respectively. These were chosen from among others based upon the more extensive self-absorption seen in other spectral lines.

The addition of the matrices SiO_2 and $CaCO_3$ to the same iron and aluminum compounds indicated the preferential use of powders. Similar slopes observed for powdered iron samples indicate the absence of any matrix effect for iron (Figure 6-2). However, when iron compounds were prepared as pellets, the slope of the graph decreased by over 40% in the presence of calcium carbonate. Similarly, no matrix effect was observed for powdered aluminum samples, whereas the presence of both matrices in pellets of aluminum samples resulted in significantly different slopes (as much as 45%).

The quantitative accuracy of the technique was determined by determining the iron content in powdered samples. Powdered samples were used because of a minimal observed matrix effect. The results in Table 6-1 are comparable (% relative errors of less than 10%) to certified values, indicating the reliability of the use of powders for accurate analysis.

Study of the influence of particle diameter on the emission signal intensity is important because of the application of LIPS to geological samples. By extrapolation of the calibration curve made from aluminum compounds, the aluminum content of Al_2O_3

particles of varying size was determined and compared to the certified value. The results from the analysis (Table 6-2) indicate a strong relationship between particle size and signal intensity. As shown, LIPS analysis was only reliable for sample particles with diameters greater than about 100 μm.

Elemental determination was also extended to the analysis of NIST SRM (National Institute of Standards and Technology – Standard Reference Material) ores. The amounts of Al_2O_3 and SiO_2 in certified ore samples were determined simultaneously. Two calibration curves were constructed from analyses of known concentrations of ore standards 691 and 693 diluted with graphite (Figure 6-3). Elemental concentrations were obtained by extrapolation of these calibration curves. For example, NIST ore 691 (1.22% Al_2O_3, 3.70% SiO_2) was diluted with graphite at various percentages: 10% 691 with 90% graphite, 30% 691 with 70% graphite, 50% 691 with 50% graphite, 70% 691 with 30% graphite, and 100% 691. Each of these concentrations could be stoichiometrically converted to the Al_2O_3 and SiO_2 concentrations, each under 4%, as shown in Figure 6-3. These samples were then prepared as either pellets or powders. This same approach was used in the calibration with NIST ore 693, resulting in the four graphs of Figure 6-3.

The results, shown in Table 6-3, indicate reasonable accuracy with samples prepared as powders, indicating the absence of any significant matrix effect. However, poorer results were obtained with samples prepared as pellets. The proposed method was applied to the simultaneous determination of Al_2O_3 and SiO_2 in ore standards. A 5.6% error for Al_2O_3 and 0.3% error for SiO_2 were achieved using powders. The small percent error observed with the use of powders relative to that obtained from the use of pellets indicates the preferential utilization of powders for this methodology. Better precision was also

achieved using powders; the RSD obtained using powders is approximately 5%, while that obtained with pellets is 8%.

Conclusion

An accurate determination of powdered geological materials was achieved by using a compact laser-induced plasma spectrometer with microscopic sample imaging. Matrix effects were evaluated by examining calibration curves constructed from analyses of iron and aluminum compounds. These compounds were presented to the laser beam in either the pressed pellet or powder form. Accurate concentrations were determined from only those samples prepared as powders, indicating the absence of matrix effects that are typically observed. Experimental results agreed well with certified values, provided the sample particle size was greater than 100 μm. Finally, the technique was able to simultaneously determine the concentrations of two different elements with reasonable accuracy. The advantageous powder sample preparation has potential for on-line, real-time analysis of raw materials for mining and chemical processing industries.

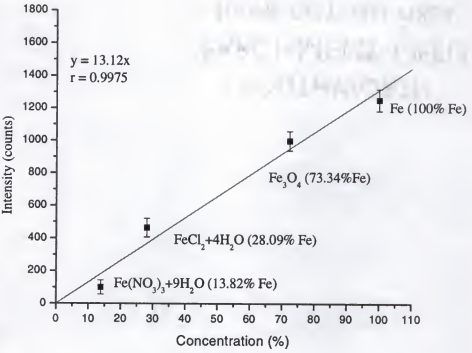

Figure 6-1. Calibration curve of iron.

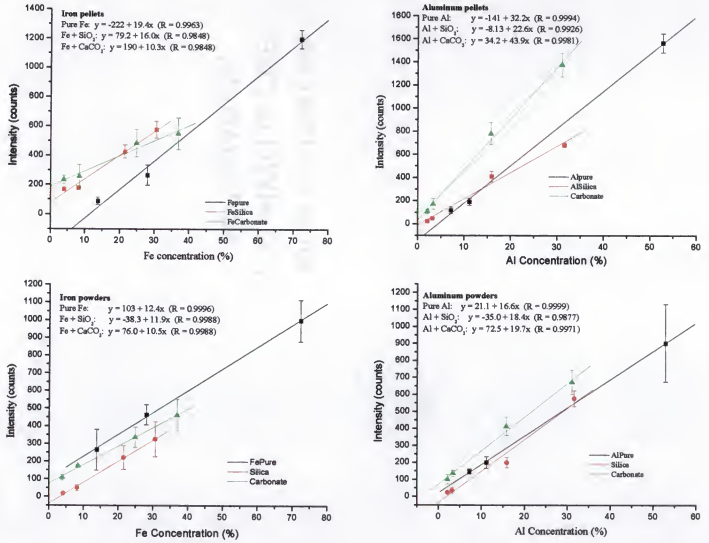

Figure 6-2. Fe & Al compounds prepared as pellets or powders.

Table 6-1. Determination of iron in ores (wavelength: 274.60 nm).

Sample	% Iron		% error
	LIPS value[†]	Certified value	
690	70.69	66.85	5.7
691	82.17	90.80	9.5
692	64.72	59.58	8.6
693	64.86	65.11	0.4

[†]Each value is an average of five shots.

Table 6-2. Determination of aluminum in particles of Al_2O_3 of different sizes (wavelength: 282.20 nm).

Particle size (μm)	% Al LIPS value†	% error
15	37.13	38.6
30	47.87	20.9
44	56.20	7.1
117	59.33	1.9
208	59.42	1.8
617	60.92	0.7

† Certified value is 60.5% Al;
each value is an average of five shots.

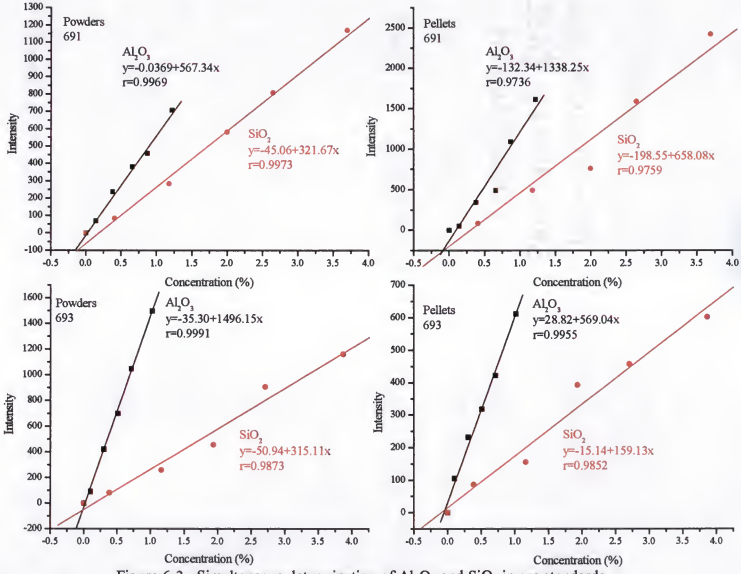

Figure 6-3. Simultaneous determination of Al_2O_3 and SiO_2 in ore standards.

Table 6-3. Simultaneous determination of Al_2O_3 and SiO_2 in ore standards.

	% Al_2O_3					% SiO_2				
Calibration with **691**	Certified value	Powder	%error	Pellet	%error	Certified value	Powder	%error	Pellet	%error
27f	0.82	0.98	19.5	1.25	52.4	4.17	3.99	4.3	3.18	23.7
690	0.18	0.24	33.3	1.31	627.8	3.71	3.64	1.9	1.98	46.7
693	1.02	1.24	21.6	1.14	11.8	3.87	3.88	0.3	1.81	53.2

Calibration with **693**	Certified value	Powder	%error	Pellet	%error	Certified value	Powder	%error	Pellet	%error
27f	0.82	1.05	28.0	1.23	50.0	4.17	4.57	9.6	6.90	65.5
690	0.18	0.17	5.6	1.55	761.1	3.71	3.76	1.3	4.59	23.7
691	1.22	1.15	5.7	1.84	50.8	3.70	4.10	10.8	14.35	287.8

CHAPTER 7
CONCLUSIONS AND FUTURE WORK

The experiments performed in this research have demonstrated the versatility of laser-induced plasma spectroscopy. Identification of materials was achieved by using the spectral "fingerprints" that are unique to each sample. LIP spectra are amenable to many types of data analysis techniques, only a few of which have been discussed in this dissertation. Several studies involved the development and evaluation of various instrumental configurations, with the goal of optimizing a configuration for use in the phosphate industry. Furthermore, LIPS was used to study the archaeological significance of certain ceramics from the first century BC. Finally, the analytical matrix effects commonly found in LIP spectra were investigated.

The correlation techniques may still be improved. The software currently under development incorporates additional parameters, such as selection of a spectral window rather using the entire spectrum for analysis. The uninformative portions of spectra (background noise, unrelated peaks, tails) may be eliminated during spectra pre-treatment to increase the probability of correct identification. The primary concern in the chemometrics realm is the enhancement of the linear and rank correlation techniques, since these are the fastest and most robust of algorithms.

Other future endeavors could include the incorporation of the principal component analysis into real-time analysis. Currently, PCA is only used in data post-treatment. It would be advantageous to combine the accuracy of PCA with a simple one-shot LIPS analysis. This computer undertaking would achieve a highly reliable LIPS

system, although its speed would be limited by the computer's processor and the program which is written. Also, additional chemometric methods may be explored, including nonparametric methods such as K-nearest neighbor and neural networks.

In the development of a LIPS instrument for the phosphate industry, it is clear that the design of the field instrument can be improved. For single shot measurements such as these, a much smaller (and potentially less expensive) laser could be used, although a commercial source for the ideal laser for this application does not presently exist. In principle, the entire field instrument could be self-contained, self-powered and no larger than the size of the present probe head. The display electronics could also be simplified and made more compact, perhaps with the use of a palmtop computer. To improve upon remote analyses at distances of 10-20 m, the engineering of a field version would be the next practical step. The main concern with the use of such an instrument in an industrial environment is eye safety.

In order to pursue the use of LIPS as a reliable tool in archaeological analysis, several experimental avenues may be explored. A number of samples from known time periods may be analyzed in order to grasp the potential of the technique in this field. The virtual non-destructiveness of LIPS is an advantage in the analysis of precious or ancient artifacts. Finally, further investigations of analytical matrix effects are necessary. The analytical signals from a multitude of compounds must be scrupulously examined.

In conclusion, the advantages of LIPS complement its flexibility and usefulness in a variety of applications. The future of LIPS in these particular applications is promising. Because of the broad applicability of the technique, the full potential of LIPS may never be realized.

APPENDIX
OPERATIONAL INSTRUCTIONS FOR THE PORTABLE LIPS PROBE

Laser Operation

Turn on the laser power supply by turning the key clockwise on the laser ICE (Integrated Cooler and Electronics). Flip the toggle switch on the probe to the "On" position. Press the "Run" button on the laser ICE when ready to acquire spectra. Ensure the PRF (Pulse Repetition Frequency) is set to "0." Press the triangular down key to change PRF to 0 if necessary. The laser will fire and a spectrum will be taken when the trigger button on the handle is depressed and the probe is set on a sample surface.

Software General Description

A program for soil layer identification is written in Visual Basic 6.0. The software combines both data acquisition and data processing functions. It allows reliable classification of three groups of soil samples, overburden, matrix, and bedrock, by using statistical correlation analysis. Linear and nonparametric rank correlations can be applied for classification of spectral data with approximately the same results.

The software offers the following options to an operator: (i) choice of number of laser shots, (ii) choice of auto or external trigger, (iii) adjustment of discrimination level, (iv) adjustment of graph scale, and (v) options regarding the visual display. Reference spectral data are stored in a library on the computer's hard drive. As soon as the laser is triggered, a new spectrum is obtained and compared to the spectra in the reference library. The software immediately identifies the ablated material as either overburden, matrix, or bedrock.

Software Operational Instruction

1. Turn on the Sony VAIO notebook computer by pressing the power button in the upper right region of the keyboard. The computer will take a few minutes before *Windows* is ready.

2. In *Windows*, use the pointing device in the middle of the keyboard to highlight the "LIPS Probe" icon. Select by clicking the left button on the bottom of the keyboard. The operational window will be displayed (Figure A-1). The program is controlled by the selection of options in the pull down menus (see below).

3. Select "Spectrometer" → "Trigger" → "External"

This allows the software to acquire spectra from the manual use of the LIPS probe. Ensure that the check mark is to the left of "External." This step is only necessary if the spectrometer was operating in the automatic mode in the previous session.

4. Set the Total number of laser shots to the number desired in the window "Number of laser shots" (Figure A-1).

5. Select "Correlation" → "Select correlation library"

An "Open" dialog box appears. Select IMC-Agrico Library (or the library of choice for correlation with a current spectrum) by clicking on it.

(To create or add to a library, see instructions on "Creating a Library or Adding to an Existing Library" below.)

6. Press "GO" and depress the trigger button on the handle of the probe. (Ensure that the laser ICE is in the "run" mode.) The software will identify the layer by highlighting the name of the layer in red and including a "!" by its identification. The resulting screen is shown in Figure A-2. A correlation summary, a list of correlation coefficients relative to each sample in the library, and a correlation plot are all displayed along with the newly

acquired spectrum. A summary of identification results can be obtained by clicking on "Correlation Statistics." The library spectrum is superimposed on the working spectrum. The colors of the two spectra can be set independently via menu option "View" and its submenus (see below). The correlation plot is depicted in the top right corner of the spectrum graph and shows graphically quality of correlation. If the correlation plot is close to a 45-degree straight line (as the one shown in Figure A-2), the correlation is good; if it is represented by a set of widely scattered dots, the correlation is poor.

Software Available Options

Changing Spectrometer Coefficients

Select "Spectrometer" → "Coefficients"

These settings should only be changed if the spectrometer inside the probe is changed. The coefficients are included on the wavelength calibration data sheet provided by Ocean Optics.

Adjusting Discrimination Level

Select "Spectrometer" → "Discrimination Level"

Enter a value between 1 and 10. A lower number indicates more sensitivity in the acquisition of spectra. However, while a higher number will prevent one from having to repeat measurements, there is a decreased chance of accurate identification with higher values.

Creating a Library or Adding to an Existing Library

Select "Library" → "Create Library"

Select "OK", then "GO"

Depress the trigger button on the probe handle to acquire a spectrum. After a new spectrum is acquired, the software prompts to a "Save As" dialog box. To create a new

library, enter a name for the new library in the "File Name" line and select "Save." To add to an existing library, select the library to which the new spectrum would be added. Enter the layer identification as "Overburden," "Matrix," or "Bedrock" in the dialog box prompting for the name of the new library member and select "OK."

Adjusting Graph Scale

Select "View" → "Scale"

Check "Autoscale" for the software to determine the graph scale automatically.

Check "Define Scale" to enter the graph scales for the x and y axes manually. Enter the desired values in each box and press "OK."

Check "Full Scale" to use the maximum (default) scale for spectral intensity.

Changing Visual Display

The operator has the capability to adjust the color of the display according to preference. Select "View," and then select the item that is desired to be changed. The color of the background, foreground, current spectrum, and the library spectrum may be adjusted.

The operator may also display a grid overlaid on the graph. Select "View" → "Grid." Vertical or horizontal lines (or both) may be displayed to more closely examine spectral lines. These lines may be solid, dashed, or dotted, and the color may of the lines may be adjusted as well.

Choosing Spectra Acquisition

The data may be acquired from the spectrometer or from data previously acquired. Choose "Spectra acquisition" and select the appropriate option. Before acquiring data with the spectrometer, it is beneficial to run some previously collected spectra (from a correlation library, for example) and to check how the software works.

Background noise

The operator may choose to acquire raw spectra or subtract the background from a spectrum. Choose "Options" and select the desired procedure. For successful correlation, however, the option "Raw spectra" must always be checked.

Correlation Analysis

A correlation library may be selected for comparison to the current spectra. The operator has the choice of selecting either a linear correlation or a rank correlation under the "Correlation" drop-down window. As a rule, correlation results for linear and rank correlations are the same, though linear correlation is processed much faster. However, rank correlation is believed to provide more trustful results. Therefore, in cases of doubtful classification, it is helpful to collect identification statistics using both linear and rank correlations.

Saving Correlation Results

The correlation results are saved automatically to the file "c:\CorrResults.txt" after each session of data acquisition/processing. This file will be rewritten upon the next session. Therefore, to save the results of each session, it is necessary to rename the file "c:\CorrResults.txt" and place it in the desired location. The corresponding prompt appears in the end of each acquisition/processing session.

Pull-down menus

1. File
    - Save
    - Save As
    - Print
    - Exit
2. Spectrometer
    - Coefficients
    - Trigger
        - Auto
        - External
    - Discrimination Level
3. Library
    - Create Library
    - Convert existing library
        - From raw to bkg subtracted
        - From one spectrometer to another
    - From OOIBASE
        - Convert single file
        - Convert incremental sequence of files
4. View
    - Scale
        - Autoscale
        - Define Scale
        - Full Scale
    - Back Color
    - Fore Color
    - Graph Color
    - Library Graph Color
    - Grid
    - Background color
    - Cut-off limits
        - Show (check)
        - Color
    - Peaks
        - Show peaks
        - Color
5. Spectra acquisition
    - From spectrometer
    - Use stored data
6. Options
    - Raw spectra
    - Auto bkg
    - Forced bkg (Routines 2-64)
    - Subtract bkg
7. Correlation
    - Select correlation library
    - Linear correlation
    - Rank correlation

Shut-down Procedure

1. Press "EXIT" in the software to exit the program.

2. Click on the "Start" menu in the bottom left corner of the screen and select "Shut Down." Ensure "Shut Down" is highlighted and select "OK." After several seconds, the computer will automatically turn off. Fold the computer until it snaps to lock.

3. Flip the toggle switch on the probe to the "OFF" position.

4. Ensure the Laser ICE is in the "STOP" mode. The light next to "STOP" should be lit.

5. Turn the key on the laser ICE counter-clockwise to turn off.

Troubleshooting

1. Avoid pressing keys in a random fashion; the software is not fully protected against unpredictable actions. Know exactly what you are doing at each step.

2. If an error is generated, the software will terminate automatically. Simply restart the software.

3. If the software continually indicates that a poor spectrum was obtained and the measurement needs to be repeated, adjust to a higher value for the discrimination level.

4. In all other cases, please contact Ben Smith or Igor Gornushkin in the Department of Chemistry at the University of Florida.

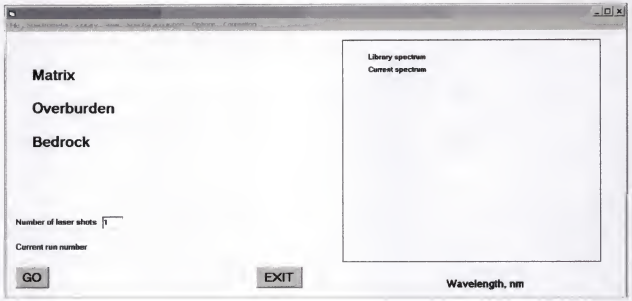

Figure A-1. View on the main menu window before any acquisition or processing of data.

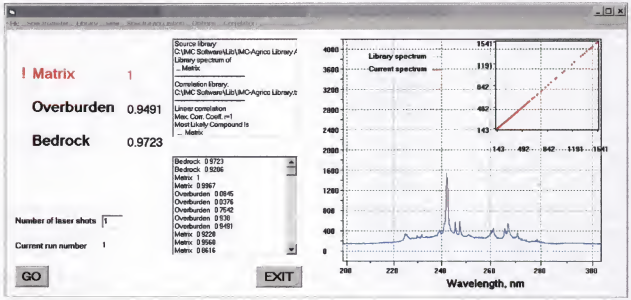

Figure A-2. Resulting screen after the data were collected and processed.

REFERENCES

1. Brech, F. and L. Cross, *Appl. Spectrosc.* **16**, 5, 1962.

2. Runge, E. F., R. W. Minck and F. R. Bryan, *Spectrochim. Acta,* **20**, 733, 1964.

3. Cremers, D. A. and L. J. Radziemski, Eds., *Laser-Induced Plasmas and Applications*, Marcel Dekker, Inc.: New York, 1989.

4. Thiem, T. L., S. Dementev, J. Melville, H. S. Melville, A. F. Kotyuk and M. Ulanovkiy, *Amer. Lab.* 20C, Nov. 1995.

5. Sneddon, J. Thiem, T. L. Lee, *Lasers in Analytical Atomic Spectroscopy*, VCH Publishers, Inc.: New York, 1997.

6. Ahmad, I. and B. J. Goddard, *Jurnal Fizik Malaysia.* **14**, 43, 1993.

7. Basov, N. G., V. A. Boiko, V. A. Gribbov, S. M. Zakharov, D. N. Krokhin and G. V. Sklizkov, *Sov. Phys. JETP*, **34**, 81, 1972.

8. Zapka, W. and A. C. Tam, *J. Opt. Soc. Am.* **71**, 1585, 1981.

9. Noll, R., R. Sattman and V. Sturm, *SPIE*, **2248**, 50, 1994.

10. Ingle, J. D. and S. R. Crouch, *Spectrochemical Analysis*, Prentice Hall: Englewood Cliffs, New Jersey, 1988.

11. Davies, C. M., H. H. Telle and A. W. Williams, *Fres. J. Anal. Chem.* **355**, 895, 1996.

12. Yamamoto, K. Y., D. A. Cremers, M. J. Ferris and L. E. Foster, *Appl. Spectrosc.* **50**, 222, 1996.

13. Cremers, D. A., M. J. Ferris, C. Y. Han, J. D. Blacic and D. R. Pettit, *SPIE*, **2385**, 28, 1995.

14. Ciucci, A., V. Palleschi, S. Rastelli, R. Barbini, F. Colao, R. Fantonic, A. Palucci, S. Ribezzo and H. J. L. Van der Steen, *Appl. Phys.* **63B**, 185, 1996.

15. Cremers, D. A., *Appl. Spectrosc.* **41**, 572, 1987.

16. Loree, T. R., *Laser Institute of America, ICALEO Conference*, Nov. 1983.

17. Radziemski, L. J., D. A. Cremers, and T. R. Loree, *Spectrochim. Acta*, **38B**, 349, 1983.

18. Davies, C. M., H. H. Telle, D. J. Montgomery, and R. E. Corbett, *Spectrochim. Acta*, **50B**, 1059, 1995.

19. Anglos, D., S. Couris, and C. Fotakis, *Appl. Spectrosc.* **51**, 1025, 1997.

20. Gornushkin, I. B., B. W. Smith, H. Nasajpour, and J. D. Winefordner, *Anal. Chem.* **71**, 5157, 1999.

21. Lehmann, E. L. and H. J. M. D'Abrera, *Nonparametrics: Statistical Methods Based on Ranks*, rev. ed., Prentice-Hall: Englewood Cliffs, NJ, 1998.

22. Anton, H., *Elementary Linear Algebra*. John Wiley & Sons: New York, 1994.

23. Lay, D. C., *Linear Algebra and Its Applications*, Addison Wesley: New York, 2000.

24. Wilson, M. J., *Clay Mineralogy: Spectroscopy and Chemical Determinative Methods*, Chapman & Hall: Oxford, U. K., 1994.

25. Wieder, M. and D. Adan-Bayewitz, *Catena*, **35**, 327, 1999.

26. Clark, R. and P. J. Gibbs, *J. Raman Spectrosc.* **28**, 99, 1997.

27. Adan-Bayewitz, D. and I. Perlman, *Archaeom.* **27**, 203, 1985.

28. Adan-Bayewitz, D. and M. Wieder, *J. Field Arch.* **19**, 189, 1992.

29. Giauque, R. D., *X-Ray Spectrom.* **23**, 160, 1994.

30. Giauque, R. D., F. Asaro, F. H. Stross, and T. R. Hester, *X-Ray Spectrom.* **22**, 44, 1993.

31. Papargyris, A. D. and R. D. Cooke, *Brit. Cer. Trans.* **95**, 107, 1996.

32. Wang, D. and D. W. Anderson, *Can. J. Soil Sci.* **80**, 251, 2000.

33. Su, C. F., S. Feng, J. P. Singh, F-Y Yueh, J. T. Rigsby III, D. L. Monts and R. L. Cook, *Glass Technol.* **41**, 16, 2000.

34. Anglos, D., S. Couris and C. Fotakis, *Appl. Spectrosc.* **51**, 1025, 1997.

35. Burgio, L., R. J. H. Clark, T. Stratoudaki, M. Doulgeridis and D. Anglos, *Appl. Spectrosc.* **54**, 463, 2000.

36. Gobernado-Mitre, I., A. C. Prieto, V. Zafiropoulos, Y. Spetsidou and C. Fotakis, *Appl. Spectrsoc.* **51**, 1125, 1997.

37. Gornushkin, I. B., A. Ruiz-Medina, J. M. Anzano, B. W. Smith and J. D. Winefordner, *J. Anal. At. Spectrom.* **15**, 581, 2000.

38. Anzano, J. M., I. B. Gornushkin, B. W. Smith and J. D. Winefordner, *Polym. Eng. Sci.* **40**, 2423, 2000.

39. Rusak, D. A., B. C. Castle, B. W. Smith and J. D. Winefordner, *Crit. Rev. Anal. Chem.* **27**, 257, 1997.

40. Eppler, A. S., D. A. Cremers, D. D. Hickmott, M. J. Ferris and A. C. Kostelo, *Appl. Spectrosc.* **50**, 1175, 1996.

41. Chan, G. C.-Y., W. T. Chang, X. Mao and R. E. Russo, *Spectrochim. Acta*, **55B**, 221, 2000.

42. Morrison, C. A., D. D. Lambert, R. J. S. Morrison, W. W. Ahlers, and I. A. Nicholls, *Chem. Geol.* **119**, 13, 1995.

43. Motelica-Heino, M., O. F. X. Donard and J. M. Mermet, *J. Anal. At. Spectrom.* **14**, 675, 1999.

44. Chaléard, C., P. Mauchien, N. Andre, J. Uebing, J. L. Lacour and C. Geertsen, *J. Anal. At. Spectrom.* **12**, 183, 1997.

45. Ciucci, A., M. Corsi, V. Palleschi, S. Rastelli, A. Salvetti and E. Tognoni, *Appl. Spectrosc.* **53**, 960, 1999.

BIOGRAPHICAL SKETCH

The author was born August 21, 1975, in Atlanta, Georgia, and spent his childhood in Stone Mountain, a suburb of Atlanta. He is the youngest child in a family that includes his parents, Florie and Delynn, and his sister, Marie, and brother, Myles. He attended Stone Mountain High School graduating with honors in 1993. He attended Berry College in Rome, Georgia, and graduated cum laude in 1997 with a Bachelor of Science in chemistry and a minor in mathematics. He studied analytical chemistry under the direction of James D. Winefordner at the University of Florida to pursue his doctoral degree.

I certify that I have read this study and that in my opinion it conforms to acceptable standards of scholarly presentation and is fully adequate, in scope and quality, as a dissertation for the degree of Doctor of Philosophy.

James D. Winefordner, Chairman
Graduate Research Professor of Chemistry

I certify that I have read this study and that in my opinion it conforms to acceptable standards of scholarly presentation and is fully adequate, in scope and quality, as a dissertation for the degree of Doctor of Philosophy.

David H. Powell
Scientist in Chemistry

I certify that I have read this study and that in my opinion it conforms to acceptable standards of scholarly presentation and is fully adequate, in scope and quality, as a dissertation for the degree of Doctor of Philosophy.

Willard W. Harrison
Professor of Chemistry

I certify that I have read this study and that in my opinion it conforms to acceptable standards of scholarly presentation and is fully adequate, in scope and quality, as a dissertation for the degree of Doctor of Philosophy.

Jon D. Stewart
Associate Professor of Chemistry

I certify that I have read this study and that in my opinion it conforms to acceptable standards of scholarly presentation and is fully adequate, in scope and quality, as a dissertation for the degree of Doctor of Philosophy.

Joseph J. Delfino
Professor of Environmental Engineering Sciences

This dissertation was submitted to the Graduate Faculty of the Department of Chemistry in the College of Liberal Arts and Sciences and to the Graduate School and was accepted as partial fulfillment of the requirements for the degree of Doctor of Philosophy.

May 2002

_____
Dean, Graduate School